(2)

AD

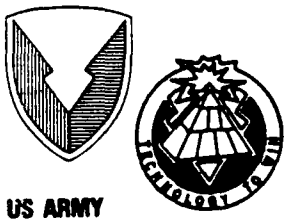

MTL TR 90-20

EFFECT OF CASTING PROCEDURES AND DIESEL ENGINE ENVIRONMENT ON THE BEHAVIOR OF ALUMINUM TITANATE

April 1990

R. J. STAFFORD, J. W. COGBURN, and T. M. YONUSHONIS
Cummins Engine Co., Inc.
Box 3005, Mail Code 50183
Columbus, IN 47202-3005

FINAL REPORT

Contract DAAL04-87-C-0085

Prepared for

U.S. ARMY MATERIALS TECHNOLOGY LABORATORY
Watertown, Massachusetts 02172-0001

The findings in this report are not to be construed as an official Department of the Army position, unless so designated by other authorized documents.

Mention of any trade names or manufacturers in this report shall not be construed as advertising nor as an official indorsement or approval of such products or companies by the United States Government.

DISPOSITION INSTRUCTIONS

Destroy this report when it is no longer needed.
Do not return it to the originator.

UNCLASSIFIED

SECURITY CLASSIFICATION OF THIS PAGE (When Data Entered)

REPORT DOCUMENTATION PAGE		READ INSTRUCTIONS BEFORE COMPLETING FORM
1. REPORT NUMBER MTL TR 90-20	2. GOVT ACCESSION NO.	3. RECIPIENT'S CATALOG NUMBER
4. TITLE (and Subtitle) EFFECT OF CASTING PROCEDURES AND DIESEL ENGINE ENVIRONMENT ON THE BEHAVIOR OF ALUMINUM TITANATE		5. TYPE OF REPORT & PERIOD COVERED Final Report - October 1987 to December 1989 6. PERFORMING ORG. REPORT NUMBER
7. AUTHOR(s) R. J. Stafford, J. W. Cogburn, and T. M. Yonushonis		8. CONTRACT OR GRANT NUMBER(s) DAAL04-87-C-0085
9. PERFORMING ORGANIZATION NAME AND ADDRESS Cummins Engine Co., Inc. Box 3005, Mail Code 50183 Columbus, IN 47202-3005		10. PROGRAM ELEMENT, PROJECT, TASK AREA & WORK UNIT NUMBERS D/A Project: 1L162105.AH84
11. CONTROLLING OFFICE NAME AND ADDRESS U.S. Army Materials Technology Laboratory, Watertown, MA 02172-0001 SLCMT-PR		12. REPORT DATE April 1990 13. NUMBER OF PAGES 89
14. MONITORING AGENCY NAME & ADDRESS(if different from Controlling Office)		15. SECURITY CLASS. (of this report) Unclassified 15a. DECLASSIFICATION/DOWNGRADING SCHEDULE
16. DISTRIBUTION STATEMENT (of this Report) Approved for public release; distribution unlimited.		
17. DISTRIBUTION STATEMENT (of the abstract entered in Block 20, if different from Report)		
18. SUPPLEMENTARY NOTES COR J. Swab		
19. KEY WORDS (Continue on reverse side if necessary and identify by block number) Aluminum titanate Casting procedures Diesel engines Mechanical properties Thermophysical properties Exhaust ports		
20. ABSTRACT (Continue on reverse side if necessary and identify by block number) (SEE REVERSE SIDE)		

DD FORM 1 JAN 73 1473 EDITION OF 1 NOV 65 IS OBSOLETE

UNCLASSIFIED

SECURITY CLASSIFICATION OF THIS PAGE (When Data Entered)

Block No. 20

ABSTRACT

The purpose of this report is to document the final results and conclusions of work on the behavior of aluminum titanate materials in a diesel engine environment. The work was conducted in three phases. Phase 1 covered investigation of material properties and microstructures of aluminum titanate materials from three different manufacturers. Phase 2 consisted of testing and evaluation of the material properties and microstructure, of each of the materials, after environmental exposures. Phase 3 work involved investigation of casting procedures to produce a cast-in-place exhaust port. Temperature profiles were recorded and different external compliant layers and core sand compositions were examined.

The aluminum titanate material from the three different manufacturers showed significant differences in strength, stability and thermophysical properties. One material was low density with low strength, modulus and conductivity. The second material exhibited degradation to α-Al_2O_3 after aging at temperatures greater than 1000° C. The third material had very high strength as-received but showed a strength loss of up to 40% after aging. However, the strength for this material after aging remained greater than the as-received strength of the other two materials.

The casting studies showed that cast-in-place ports can be produced. The most promising results were seen when the core sand composition was 50% SiC/ 50% Fe. This composition had thermal expansion characteristics which kept the core sand in contact with the aluminum titanate port during solidification and cooling of the cast iron. However, the casting parameters must be optimized to improve the success rate for casting-in-place.

The successful production of cast-in-place exhaust ports is a significant challenge. Major time and financial investments will be required to fully understand and implement the required changes to the cylinder head, port design, materials and casting procedures.

Table of Contents

Table of Figures

Table of Tables

INTRODUCTION:

Cummins Engine Company has been involved in the development of cast-in-place aluminum titanate exhaust ports since 1983. In the last five years, Cummins, Coors Ceramic, Case Western Reserve University, and Golden Foundry have been developing the methodology to incorporate insulating ceramic exhaust ports into advanced diesel engines. Through this work, Cummins Engine Company has characterized three suppliers of aluminum titanate ceramics.

Applications for ceramic materials in the exhaust port have been investigated since 1976 when studies by Ford [1,2] showed that low heat rejection in the exhaust port could improve the catalytic converter efficiency and reduce cooling system size in a spark ignition engine. Subsequent studies and modelling by Ricardo [3] and Cummins [4] on direct injection diesel engines reported that approximately 30% of the heat rejected to the coolant comes from the exhaust port. These studies determined that insulation of the port results in a 30 to 50% decrease in the heat rejection to the coolant from the port, thus, resulting in a 10 to 15% decrease in total engine heat rejection to the coolant.

The reasons for adding an insulated exhaust port to an engine are two-fold. The thermal energy in the exhaust gas does not transfer into the cylinder head resulting in lower heat rejection to the coolant system and the opportunity to reduce the size of the coolant system. The thermal energy retained in the exhaust gas is then used in the turbocharging system to provide a higher boost pressure for the intake air to the cylinder resulting in an increase in engine output power.

Aluminum titanate is being investigated for use as exhaust port liners in diesel engines because the material has a favorable combination of properties that will allow a component to survive the thermal and mechanical stresses of casting and provide long life in the end use application. Aluminum titanate exhibits desirable thermal properties of low thermal conductivity, low apparent thermal expansion and excellent thermal shock resistance. The low thermal expansion results from extreme anisotropy in the crystal structure and microcrack formation at the grain boundaries.[5] The extent of microcracking is a function of grain size [6] and can significantly reduce the strength and modulus of the aluminum titanate.

This material has been in commercial production at Porsche in Europe [7] since 1985 for spark ignition engines. The successful application of insulating exhaust ports by Porsche has proven that improvements in thermal efficiency, pollution control and cooling system size are possible.[8] However, incorporating insulating exhaust ports in a cast iron cylinder head for a commercial diesel engine remains a formidable challenge.

In the case of heavy duty diesel engine heads, the head material is gray or ductile iron with a much higher pouring temperature than aluminum, and the heavy duty diesel engine ports themselves are approximately 2 to 3 times larger than automotive ports. These two items, coupled with the higher strength of iron, results in fracture of the aluminum titanate ports.

Casting models have been developed [9,10] to aid in design of components which will survive the casting process. However, review of available information, including results of this work, by Cummins, Coors Ceramic, Hoechst, NGK Insulators, Case Western and others, has indicated that changes in the aluminum titanate material properties and/or changes in design geometry, by

themselves, are not sufficient to obtain successful castings for diesel engine applications. Cummins has shown through their internal studies that compliant layers on the outside of the ports and that reducing the thermal expansion mismatch during cooling, between the core material and cast ductile iron, can significantly improve the survivability of the port. Cummins has also shown that the port casting survivability depends in part on the thickness of the metal, pour temperature, and the core material to mention a few variables that appear significant.

This work was conducted in three phases, with each phase examining different aspects of the material properties or casting performance. Phase I involved a study of aluminum titanate material properties as-received, after simulated casting and actual casting conditions. Phase II involved a study of aluminum titanate material properties after long term exposure to simulated exhaust conditions. The material properties in Phases I and II were studied with the application of cast-in-place diesel exhaust ports in mind. The most important properties to consider include material microstructure, thermal expansion and thermal conductivity in regard to the thermal behavior during the application. Mechanical properties of the material are also important in terms of the casting operation and the long term durability of the insulated diesel engine head. Phase III involved casting aluminum titanate ports into cast iron and examination of the effects of compliant layers and core sand composition on the survival of the port during the casting process.

EXPERIMENTAL PROCEDURE:

Aluminum titanate from three different sources was subjected to the following exposures and tests to evaluate the material properties and performance as related to use in a diesel engine exhaust port liner. The three suppliers of aluminum titanate for this work were Coors Ceramic, Hoechst Ceramatec and NGK Insulators.

ENVIRONMENTAL EXPOSURE

The aluminum titanate materials being investigated were subjected to different environmental exposures to examine the material property behavior under conditions similar to those expected in production and during the service life.

Phase I

The purpose of the exposures in Phase I of the program was to examine the effects of simulated and actual casting environments on the material properties.

Thermal Exposure

Test bar specimens of each aluminum titanate were exposed in an oxidizing furnace environment for 15 minutes at 1370°C and then furnace cooled to room temperature. This exposure was designed to simulate the thermal stresses induced in the material from thermal shock at the 1370°C pour temperature for molten iron and subsequent thermal contraction stresses as the iron casting solidifies and cools to room temperature.

Casting Exposure

Generic design exhaust ports and flat plates of each aluminum titanate were cast into ductile iron blocks. The initial pour temperature of the molten iron was 1425°C with cooling to 1370°C during the pour.

Thermal Degradation Exposure

The thermal degradation behavior of each of the aluminum titanates was examined. Specimens cut from flat plates, as-received and after casting exposure, were heated from 25°C to 980°C in 5 h, held at temperature for 5 h, and furnace cooled.

Phase II

The purpose of Phase II of the program was to examine the effects of long term thermal exposure of the materials in an thermal environment representative of anticipated exhaust port operation temperatures.

Thermal Exposure

Test bar specimens were exposed to a simulated casting temperature of 1370°C. One sample set, Lot A, was exposed for 30 min and a second sample set, Lot B, was exposed for 24 h. Following the casting temperature exposure, both sample sets were divided into four groups and each group of specimens held at simulated engine exhaust gas temperatures for 500 h. These temperatures are as follows:

Baseline (#1)	No additional exposure
Exposure #2	540°C
Exposure #3	815°C
Exposure #4	1090°C

The temperatures chosen for the exposures were determined from the current and anticipated exhaust gas temperatures from the power cylinder. Exposure #2 represents the current average exhaust gas temperature for a diesel engine. Exposure #3 represents the anticipated exhaust gas temperature from an insulated power cylinder and exposure #4 represents the surface temperature of the insulated components in the combustion zone.

Diesel Exhaust Exposure

Two sets of test bar specimens for each of the aluminum titanates were exposed to a simulated casting temperature of 1370°C. One set of specimens was exposed for 30 min and the second set was exposed for 24 h. Following the simulated casting exposure, the specimens were placed in the exhaust stream of an operating diesel engine for 500 hours.

Cylinder Head Casting

A V-903 production multi-cylinder head was cast at Golden Foundry using Coors aluminum titanate exhaust ports. The core sand for the castings was SiC. Three compliant layers were placed on the ports. Two ports had a hollow ceramic sphere layer, three ports had a ceramic cement layer and three ports had a foamed ceramic layer. The pour temperature of the iron was 1425°C.

MATERIAL PROPERTY TESTING

Density

Ten test bar specimens for each of the aluminum titanates were measured with a Sylvac digital caliper and weighed on a Mettler precision analytical balance. The geometric density was calculated for each specimen and a mean sample density determined for each of the aluminum titanates.

Mechanical Properties

The mechanical properties of the aluminum titanates were investigated in the as-received condition and after the environmental exposures.

Flexural Strength

Flexural strength testing was conducted using an Instron universal testing machine. Specimens from Phase I exposures were tested in four point flexure in accordance with MIL-STD-1942(MR). Specimens from Phase II exposures were tested in three point flexure in accordance with MIL-STD-1942(MR).

Fractography

Fracture surfaces of each of the specimens from the flexural strength testing were examined optically using a Zeiss Axiomat research metallograph.

Modulus

Measurements of the elastic modulus, shear modulus and Poisson's ratio were conducted at Oak Ridge National Laboratory by Mr. Bill Simpson and Dr. Ray Johnson using an ultrasonic elastic modulus method. (See Appendix A).

Microstructural Analysis

The microstructure of representative specimens for each aluminum titanate, as-received and after each exposure, was examined using optical and X-ray techniques.

Microstructure

Specimens of each of the aluminum titanates, as-received and after each exposure, were mounted and polished. The microstructures were then examined using a Zeiss Axiomat metallograph. The fracture surface of specimens of each aluminum titanate, as-received and after the Phase I thermal exposure (1370°C/15 min, furnace cool) and as manufactured surface of specimens of each aluminum titanate, as-received and after Phase I casting exposure, were examined. The surfaces of interest were sputter coated with gold and the microstructure of each specimen examined using an Amray Scanning Electron Microscope (SEM).

Elemental and Phase Composition

The specimens examined in the SEM for microstructure were then examined for overall elemental composition and phase elemental composition using an EDAX Energy Dispersive X-ray analyzer.

X-ray Diffraction

The crystalline phase structure for representative specimens of each aluminum titanate, as-received, after casting and after thermal degradation exposure, was examined using a Siemens X-ray diffactometer. In addition, a specimen of the Hoechst material, after Phase II thermal exposure #4, was examined when results of the microstructure examination and thermal expansion tests showed that further investigation was needed.

Thermal Expansion

The thermal expansion of each aluminum titanate was measured using a Harrop Laboratories Thermal Dilatometer. The expansion was measured over the temperature range 25 to 1350°C, both heating and cooling, for as-received and Phase I exposures. The expansion was measured over the temperature range 25 to 1000°C, both heating and cooling, for Phase II exposures.

Thermal Conductivity

Thermal conductivity was measured by the Thermophysical Properties Research Laboratory (TPRL) at Purdue University. The laboratory experimentation was performed by Dr. R. E. Taylor, Director and his associates, H. Groot and J. Larimore. Two samples of Coors, Hoechst and NGK aluminum titanate and two samples of cast iron from Golden Foundry. The ceramic samples were cut from as-received plates and the cast iron samples were cut from finished castings. The Laser Flash Method for determining thermal conductivity was performed by TPRL. (See Appendix B).

CASTING

Cummins investigated the feasibility of the cast-in-place ceramic port concept in conjunction with foundry technologists at Golden Foundry and Case Western University. Most of the effort has been through trial and error processes. Instrumented casting trials were initiated to gather information concerning the actual casting process and provide a database for future modelling studies.

Preliminary Casting

Initial casting studies were conducted at Case Western University. The initial studies gave insight into the thermocouple placement on the ports, compliant layer considerations and core material considerations for the final casting studies.

Final Casting

Eight casting trials were conducted at Case Western University. Two different types of compliant layer conditions and four different core sands were investigated. Four of the castings contained no compliant layer and four contained a paper (Fiberfrax®) compliant layer. The four core sand materials investigated included SiO_2, $ZrSiO_4$, SiC and 50% SiC/50% Fe.

RESULTS:

PHASE I: MATERIAL PROPERTY EVALUATION

The Phase I work was conducted on samples of the aluminum titanate from each of the three sources in an as-received condition, after actual casting operations and after simulated casting conditions. In addition, the possible thermal degradation of Al_2TiO_5 at 980°C was investigated.

Density

The densities of the materials evaluated in this work are shown in Table 1.

Table 1: Density of Selected Aluminum Titanate Materials

Material Supplier	Density (g/cm^3)
Hoechst	3.23
Coors	3.14
NGK	2.98

Mechanical Properties

Flexural Testing

The flexural strength of as-received specimens and specimens after Phase I thermal exposure (1370°C/15 min, furnace cool) is shown in Figure 1. This data shows that in the as-received condition, the Coors material is the strongest followed by the Hoechst material and the weakest material is the NGK material. After furnace exposure, the relative ordering is unchanged. The Coors material shows a 43% loss in flexural strength after the furnace exposure, however, the after exposure strength is greater than the as-received strength of the NGK or Hoechst materials.

Fractography

Fracture surfaces of each of the specimens from flexural testing above, were examined under an optical microscope to determine fracture origins. The low strength of the materials and porosity in the microstructure made fracture origin determinations very difficult and no conclusions could be drawn from the examination.

Modulus

The results of the modulus testing are given in Table 2. The moduli for each aluminum titanate material were essentially unchanged by the casting process. Variations in measurements, due to sample inhomogeneity, were greater than the measured variations between the as-received and cast samples. The standard error for Poisson's ratio is greater than 200% due to the wide scatter in the measured values.

Figure 1: Baseline Flexural Strength of Aluminum Titanates

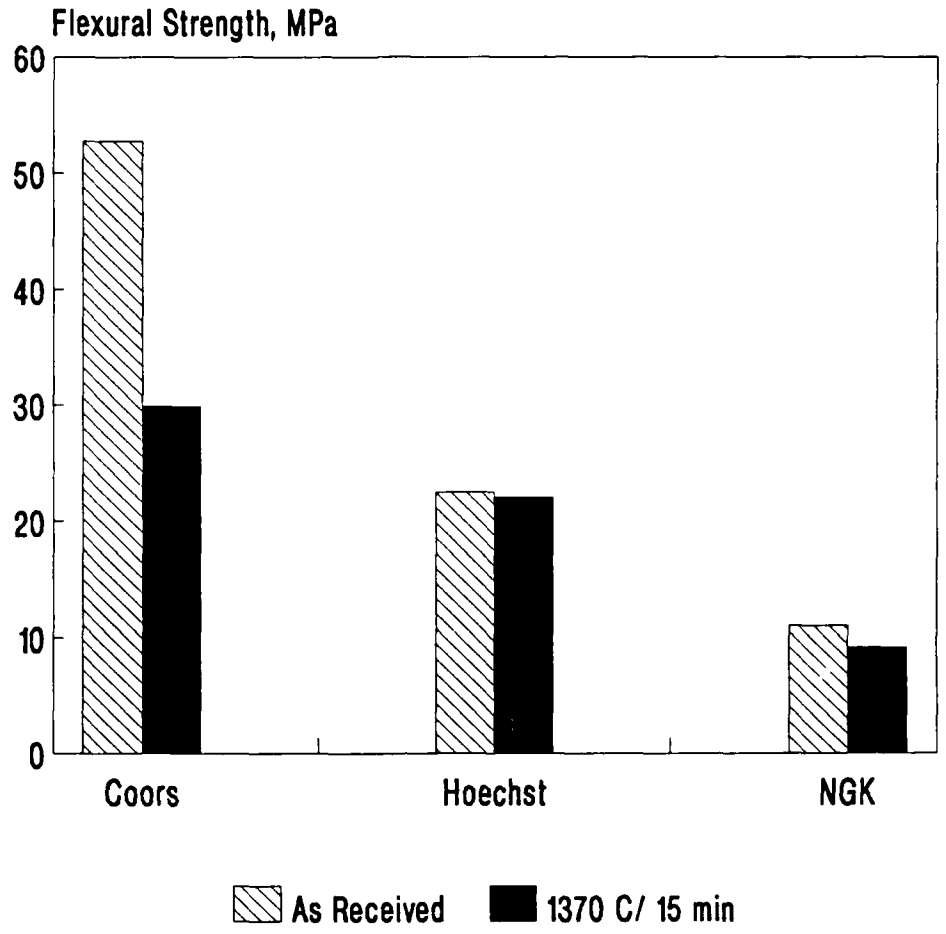

Table 2: Elastic and Shear Moduli and Poisson's Ratio

Material Supplier	Condition	Elastic Modulus (GPa)	Shear Modulus (GPa)	Poisson's Ratio
Coors	As-received	47.7	20.5	0.16
	Cast	50.0	21.2	0.18
NGK	As-received	9.3	4.4	0.06
	Cast*	10.7	5.0	0.07
Hoechst	As-received	33.5	15.2	0.10
	Cast	33.5	15.2	0.10

* - Average of two samples.

Microstructural Analysis

Microstructure

The microstructures obtained from fracture surfaces of the three materials in the as-received condition are shown in SEM photographs in Figure 2. The fine grain microstructure of the Coors material is distinctly different from the coarser grained, dense structure of the Hoechst material. The NGK material is similar to the Hoechst material with a coarser grained structure as well.

Figure 3 shows SEM photographs of the fracture surface microstructures for the three materials after initial furnace exposure of 1370°C for 15 minutes and furnace cooled, followed by 500 hours of exposure at 550°C. The fine grained microstructure of the Coors material appears to have experienced some consolidation, whereas the NGK and Hoechst materials appear relatively unchanged after exposure.

The final set of microstructures studied are shown in Figures 4 and 5, which compare all as-received and the cast Coors, NGK and Hoechst materials. In these micrographs, the as-received and Hoechst cast samples were cut from plates (machined surface), and the cast Coors and NGK samples were cut from ports (slip cast surface). Figure 4 shows the SEM photographs and Figure 5 shows the optical photographs of the polished surfaces. The NGK material was very friable and particles pulled out of the surface during polishing. This result was visible in the structure seen in both Figures 4 and 5.

As was seen in the furnace exposure, there appeared to be consolidation of the fine grained Coors material, however, the microstructure difference may also be due to the comparison of slip cast and machined surfaces. The NGK and Hoechst materials appear unaltered by exposure to the casting operation. In addition, a considerable amount of microcracking exists in the NGK aluminum titanate which may explain the lower observed strength of this material.

Figure 2: Microstructure of As-Received Materials

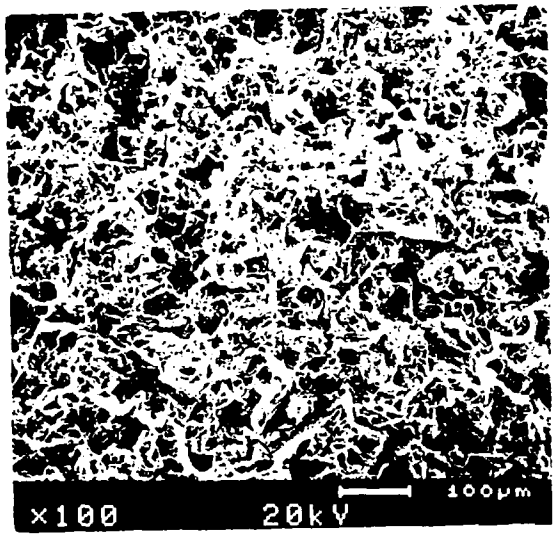

Hoechst

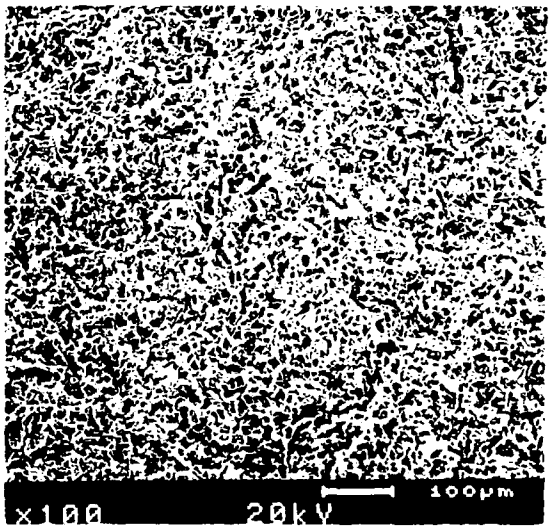

Coors

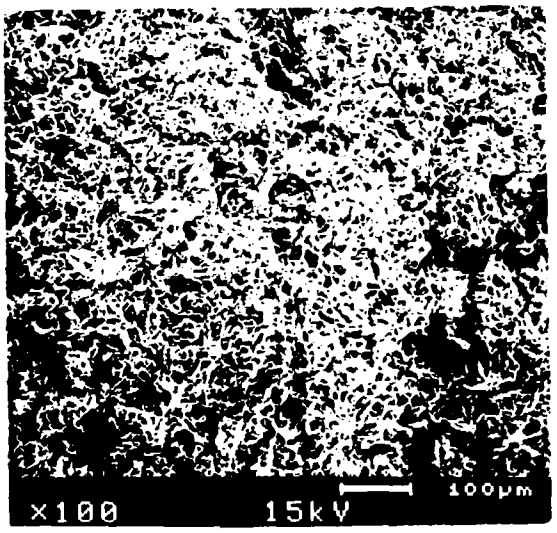

NGK

Figure 3: Microstructure After Furnace Exposure

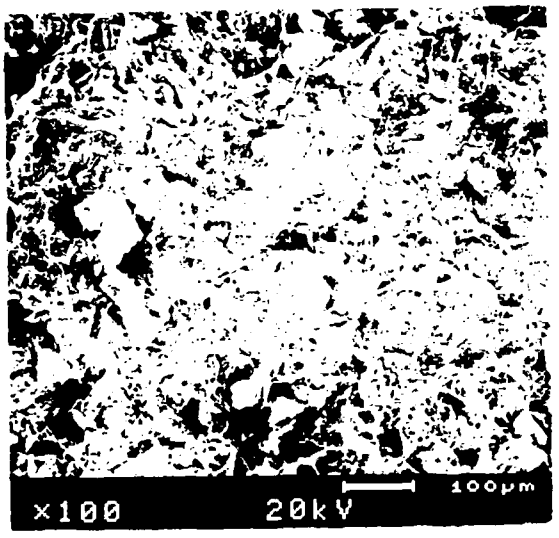

Hoechst

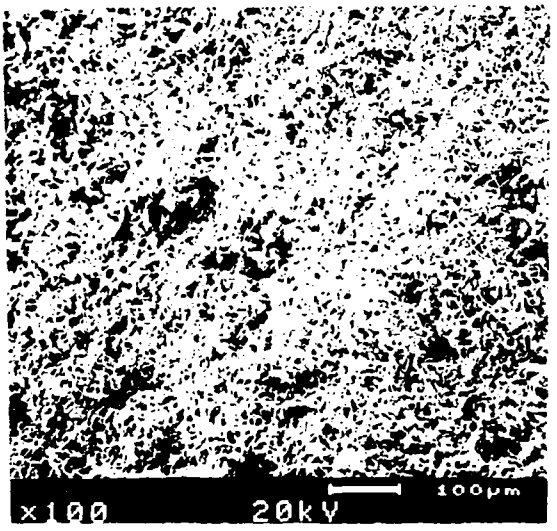

Coors

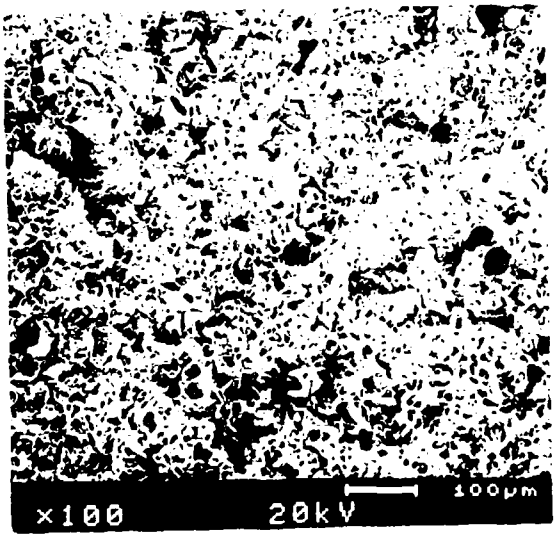

NGK

Figure 4: As-Received vs Cast Microstructure (SEM)

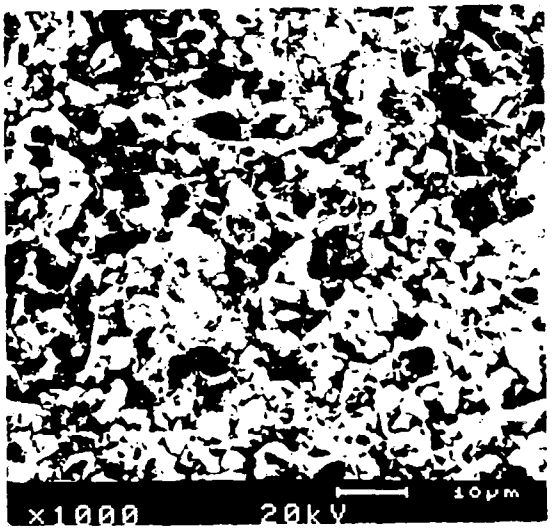

Coors As-Received

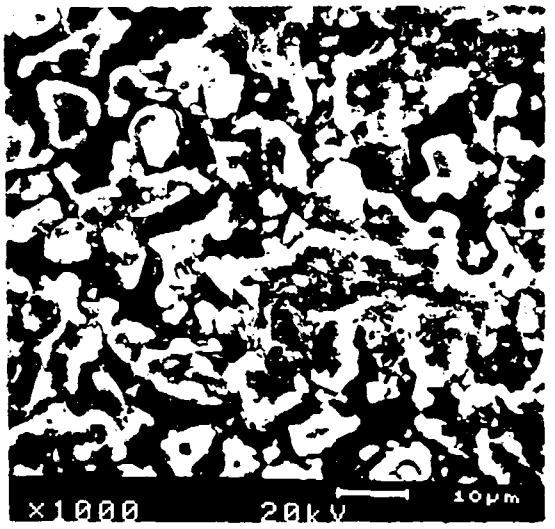

Coors After Casting

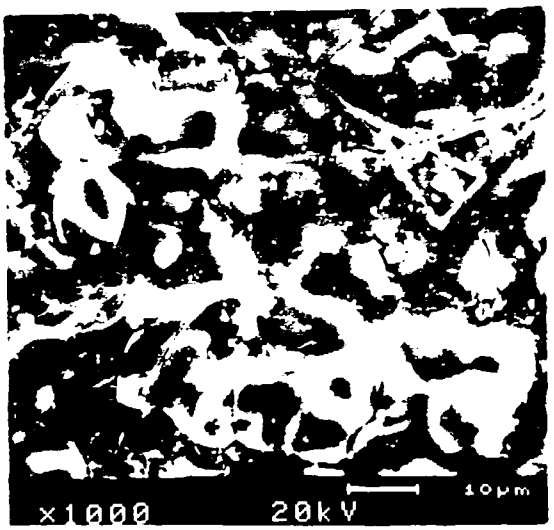

NGK As-Received

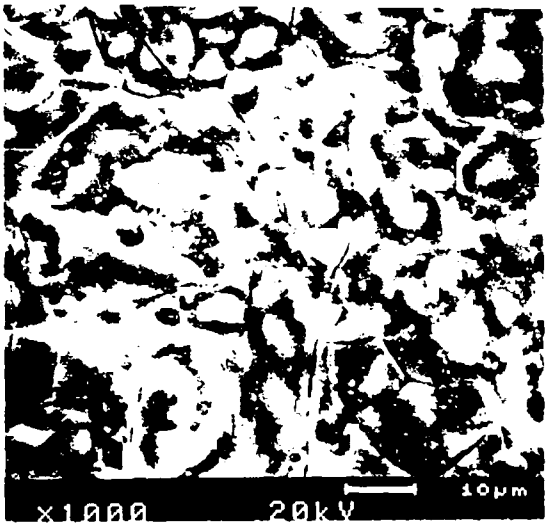

NGK After Casting

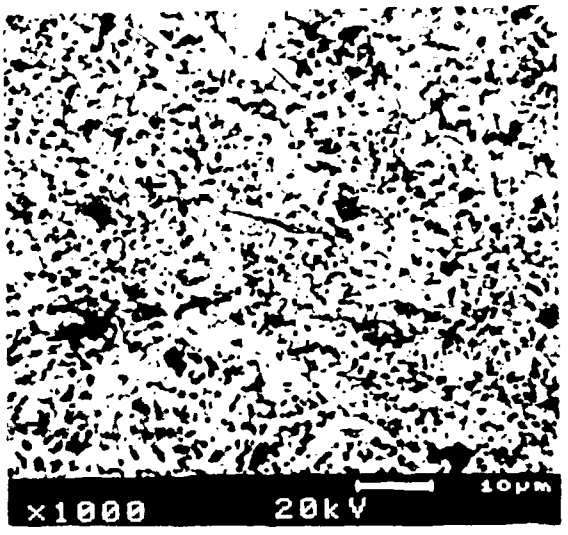

Hoechst As-Received

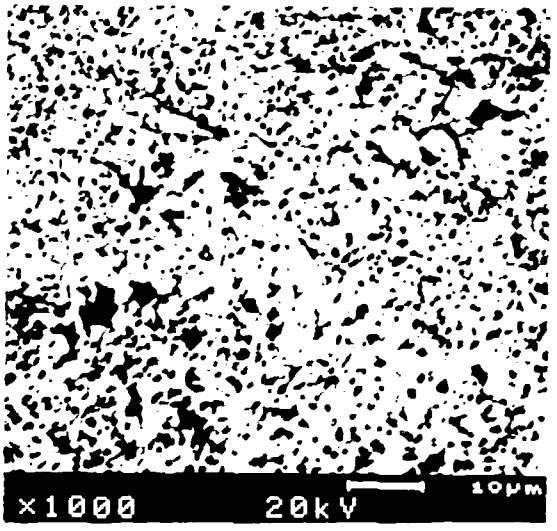

Hoechst After Casting

Figure 5: As-Received vs Cast Microstructure (Optical)

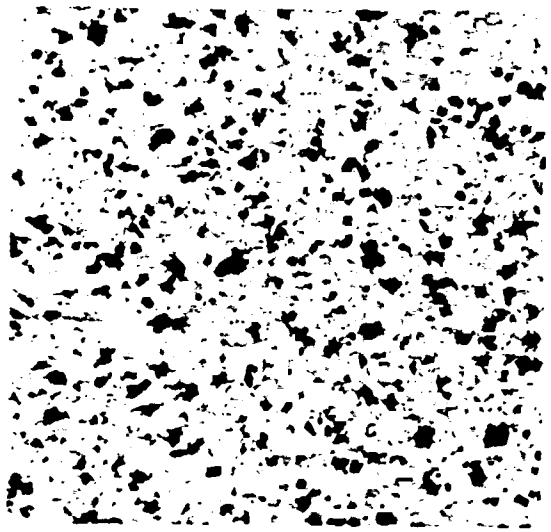

Coors As-Received
100X

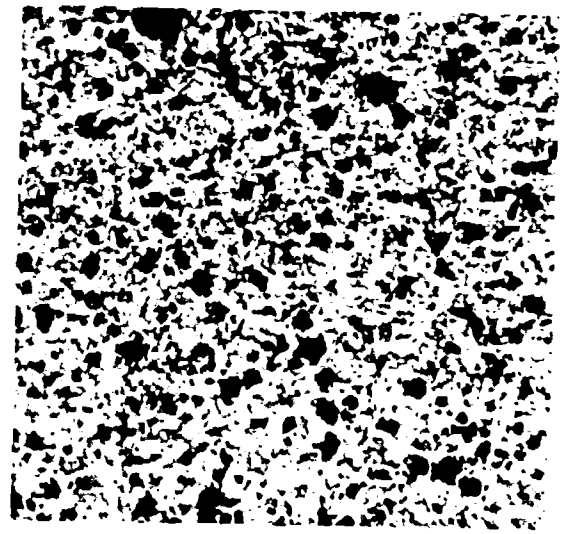

Coors After Casting
100X

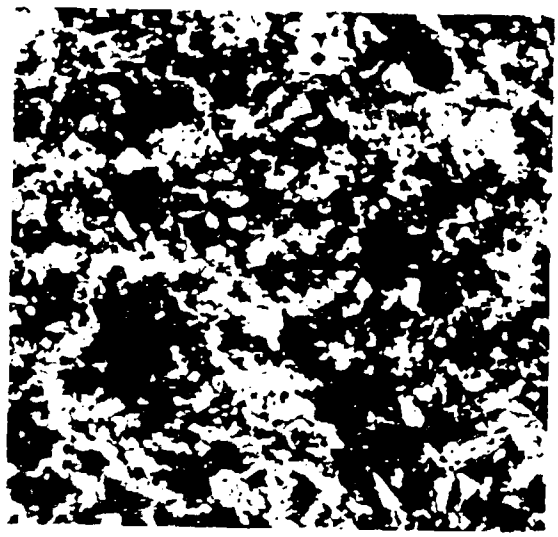

NGK As-Received
100X

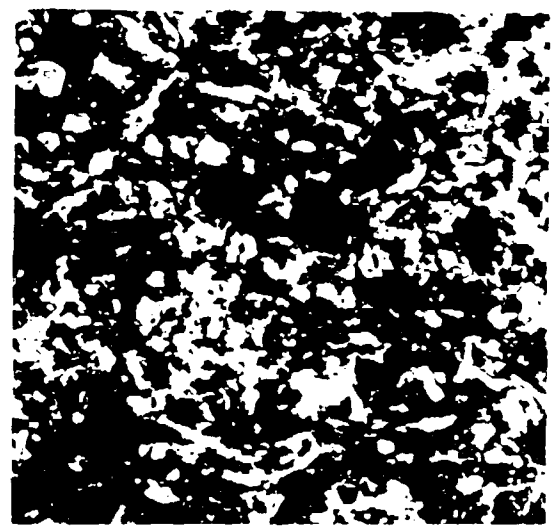

NGK After Casting
100X

Hoechst As-Received
100X

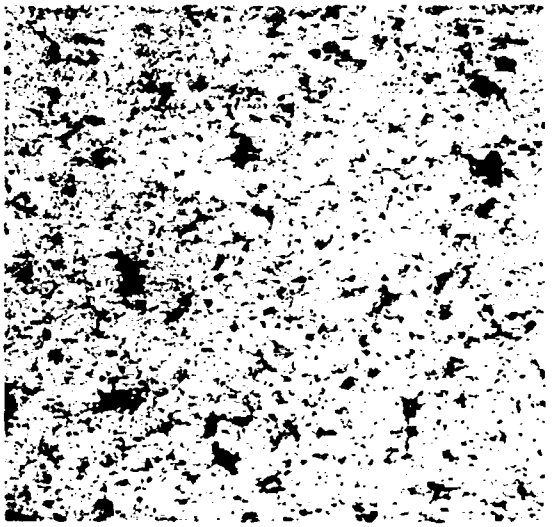

Hoechst After Casting
100X

Elemental and Phase Composition

The Coors material consists of Al, Si, Ti and Fe. The NGK material consists of all of these plus an additional quantity of Mg in the matrix. The Hoechst material consists of Al, Si, Ti and Mg.

The overall elemental concentrations and the elemental concentrations for the individual phases of each of the materials are shown in Table 3.

The microstructures of these materials exhibit three major phases, with one phase being a distribution of porosity within the structure. SEM Energy Dispersive Analysis of the phases was conducted with the following results.

The compositions of the individual phases indicate that the white phase is a titanium rich phase. In the Hoechst material this phase appears to correspond to free titania (TiO_2). In the NGK and Coors materials, the white phase appears to be predominantly Al_2TiO_5. The presence of Mg in the white phase of the NGK appears to cause some depletion of the Al content in the phase. The dark phase in the Coors and NGK materials appears to have Si substituting for Ti in the crystal structure.

The Hoechst material may contain three phases, free TiO_2, Al_2TiO_5, and Si substituted Al_2TiO_5 phases. The extreme brightness of the TiO_2 phase resulted in poor differentiation of the possible Al_2TiO_5 and Si substituted Al_2TiO_5 phases. This explains why the Hoechst dark phase composition is the same as the overall composition and much different from the Ti depleted dark phases of the NGK and Coors materials.

The data for the cast materials reveals very little difference between the composition of the phases in the as-received materials. It was expected that the phases near the interface of the casting surface would be richer in Fe, but no penetration of iron was observed.

X-ray Analysis

Previous x-ray diffraction studies on samples of as-received Coors, NGK and Hoechst aluminum titanate showed they were nearly identical.[11] This information is shown in Figure 6. Additional work was conducted to show the x-ray diffraction of the materials after casting. Figure 7 shows the after casting patterns for the Coors, NGK and Hoechst materials. The Coors and Hoechst patterns remain relatively unchanged from those of the as-received patterns. However, the NGK pattern reveals a reversal of the relative intensities between the [153] and [063] planes. The reason for this occurrence is likely to be due to oxide additions (FeO, MgO, SiO_2) to the aluminum titanate to stabilize the Al_2TiO_5 and inhibit decomposition to α -Al_2O_3 and rutile TiO_2.

Table 3: Elemental Composition of Aluminum Titanate Phases

			ATOMIC % COMPOSITION				
SAMPLE	CONDITION	PHASE	Al	Ti	Si	Fe	Mg
Coors	As-received	Overall	52.7	30.2	14.1	3.0	
Coors	As-received	Al_2TiO_5#	55.1	6.1	37.7	1.2	
Coors	As-received	Al_2TiO_5	56.3	41.9		1.7	
Coors*	Cast	Overall	54.7	30.4	11.7	3.1	
NGK	As-received	Overall	46.2	38.0	4.7	3.9	7.1
NGK	As-received	Al_2TiO_5#	62.8	2.8	33.7	0.6	
NGK	As-received	Al_2TiO_5	47.0	43.0		4.0	6.0
NGK*	Cast	Overall	48.4	39.6	3.2	3.8	5.0
Hoechst	As-received	Overall	55.6	18.4	16.6		9.5
Hoechst	As-received	Al_2TiO_5	56.1	16.2	16.1		11.6
Hoechst	As-received	TiO_2	15.5	59.3	25.5		
Hoechst*	Cast	Overall	54.8	18.0	19.1		8.1

* - Analysis of individual phases in cast materials revealed no significant difference from as-received materials.

- Al_2TiO_5 structure with Si substitution into the crystal lattice.

Examination of the x-ray diffraction patterns after thermal degradation testing (5 h at 980°C) showed that there was no change in the crystal structure of the Coors and NGK as-received and cast materials. However, the x-ray diffraction patterns for both the Hoechst as-received and cast materials showed crystal structure changes.

A representative x-ray diffraction pattern of the Hoechst material after thermal degradation is shown in Figure 8. When compared to the as-received x-ray diffraction pattern in Figure 6, the thermal degradation pattern shows an additional peak at 29° (2θ) and a reduction in the intensity of the peak at 32° (2θ). The phases identified for this pattern are the parent material, Al_2TiO_5, and a rutile TiO_2. The additional peak forms a doublet with the primary Al_2TiO_5 peak at 27° and the primary TiO_2 peak at 29°.

Figure 6: As-Received X-Ray Diffraction Patterns

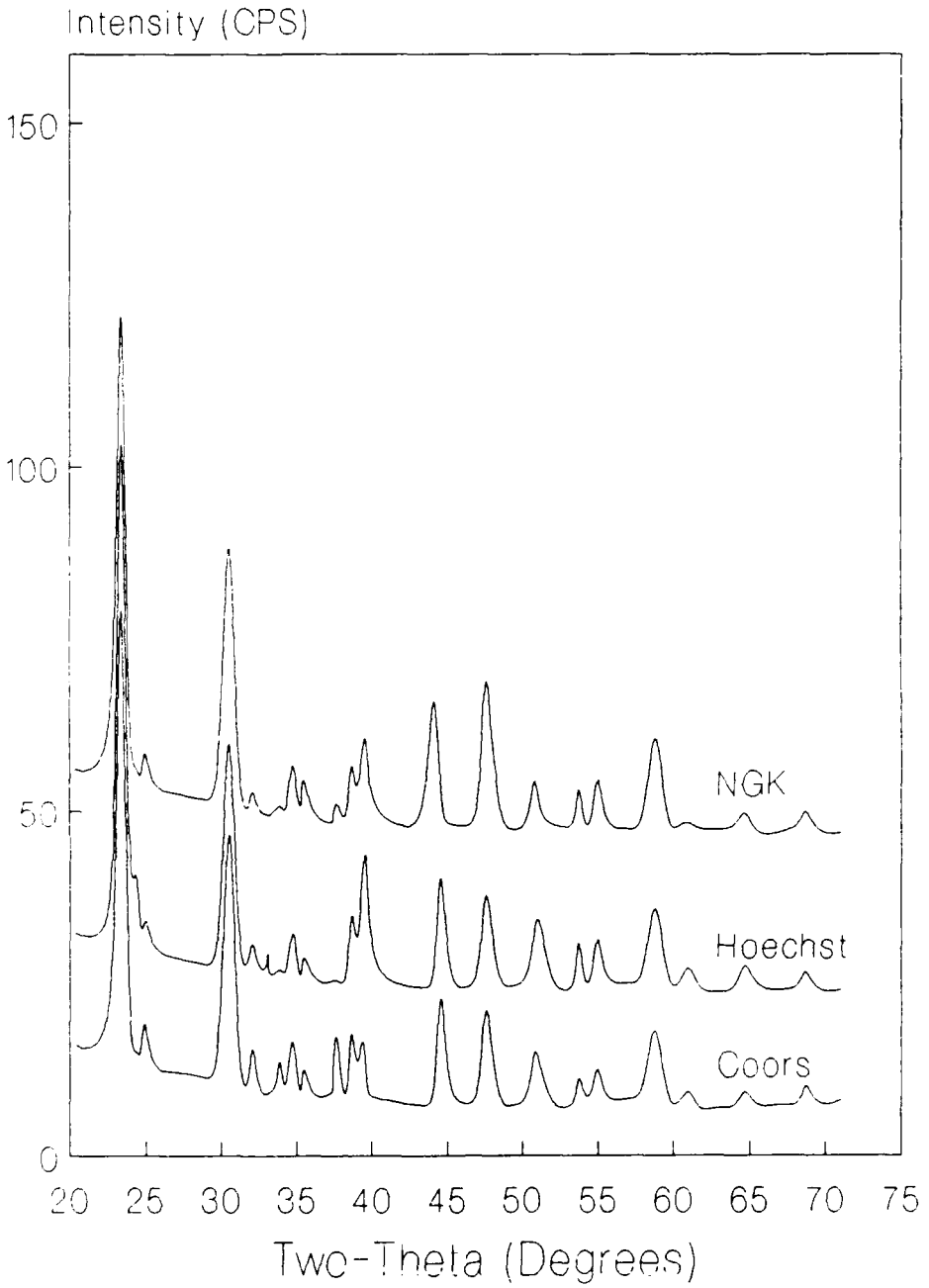

Figure 7: Cast X-Ray Diffraction Patterns

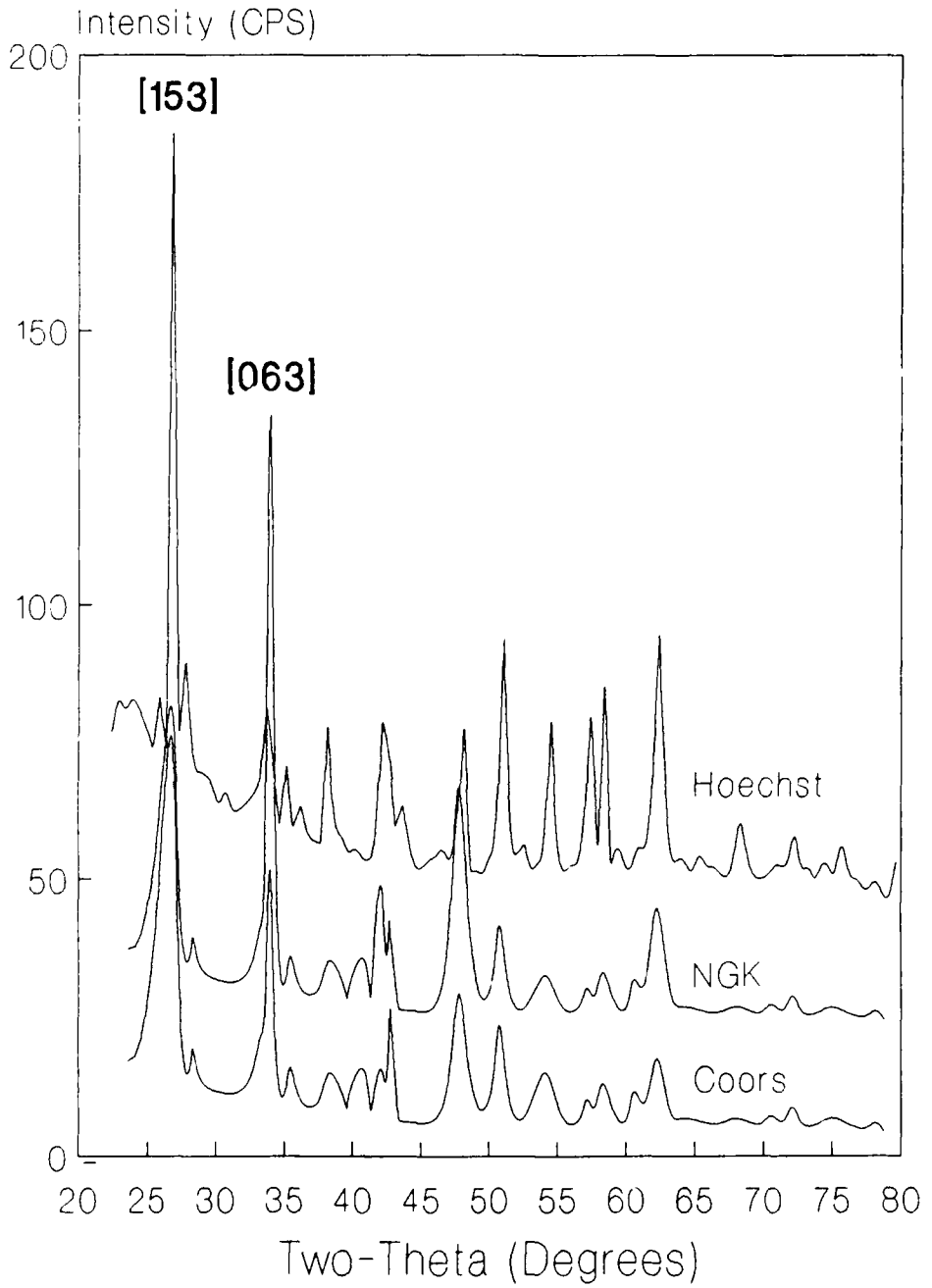

Figure 8: Hoechst Thermal Degradation X-Ray Diffraction

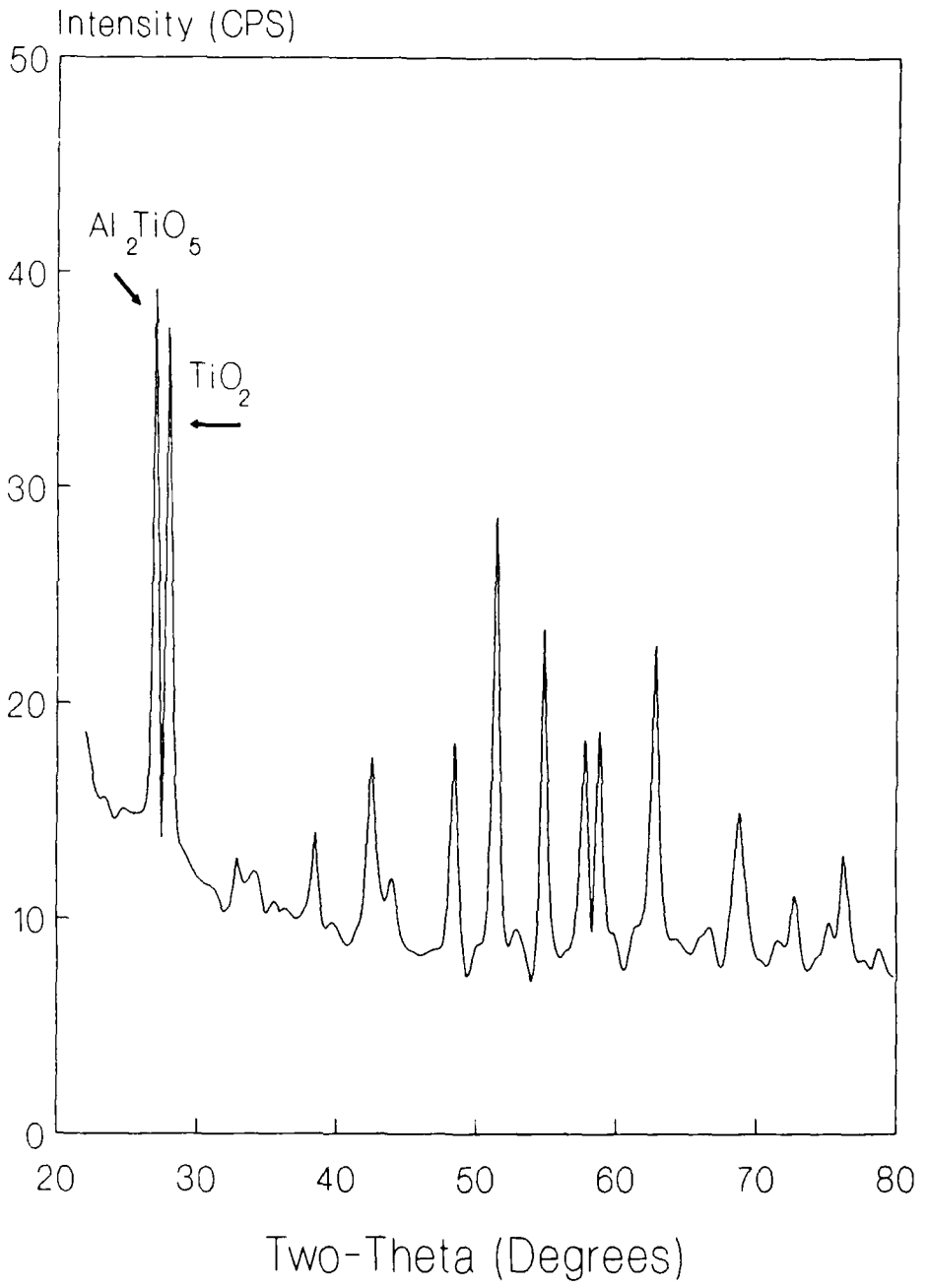

Thermal Expansion

In this section, the thermal expansion of aluminum titanate is discussed as well as the thermal expansion of cast ductile iron material from Golden Foundry.

Figure 9 shows the thermal expansion curves, from room temperature to approximately 1350°C, for as-received samples of all three of the aluminum titanate materials. The overall shape of each of the patterns is very similar, with the expected hysteresis loop. However, the NGK material appears to have undergone a permanent increase and the Hoechst material a permanent decrease in overall length. The Coors material returned to its original length.

Figure 10 shows the thermal expansion curves, from room temperature to approximately 1350°C, for the cast samples of each aluminum titanate. The cast NGK and Hoechst samples show the same behavior as the as-received samples, with the NGK undergoing a permanent increase and the Hoechst undergoing a permanent decrease in length. The behavior of the cast Coors material differs from the as-received in that the cast sample shows a permanent increase in length.

The thermal expansion of the cast iron material from Golden Foundry is shown in Figure 11. This data reveals that the Austenite-Ferrite transformation range is much different during cooling than on heating. The cooling rate in the casting will determine whether the ferrite structure is bainitic or pearlitic, and whether there is a transformation to martensite.

The thermal expansion of as-received and cast samples were examined in thermal degradation testing (5 h at 980°C). The results of this test showed that these specific test conditions did not affect the thermal expansion of any of the as-received or cast aluminum titanates.

Thermal Conductivity

Figure 12 shows the thermal conductivity data for all of the aluminum titanates. The Coors and Hoechst data show similar conductivity behavior, while the NGK reveals a much lower conductivity with a similar trend of increasing conductivity with increasing temperature.

The data for the cast iron is shown in Figure 13. One of the cast iron samples reveals behavior typical of cast iron showing a discontinuity through the transformation range just above 700°C. The other cast iron sample does not show this effect and reveals a much lower conductivity. This behavior is more typical of an alloyed steel, where the crystal structure transformations are suppressed.

Figure 9: As-Received Thermal Expansion Curves

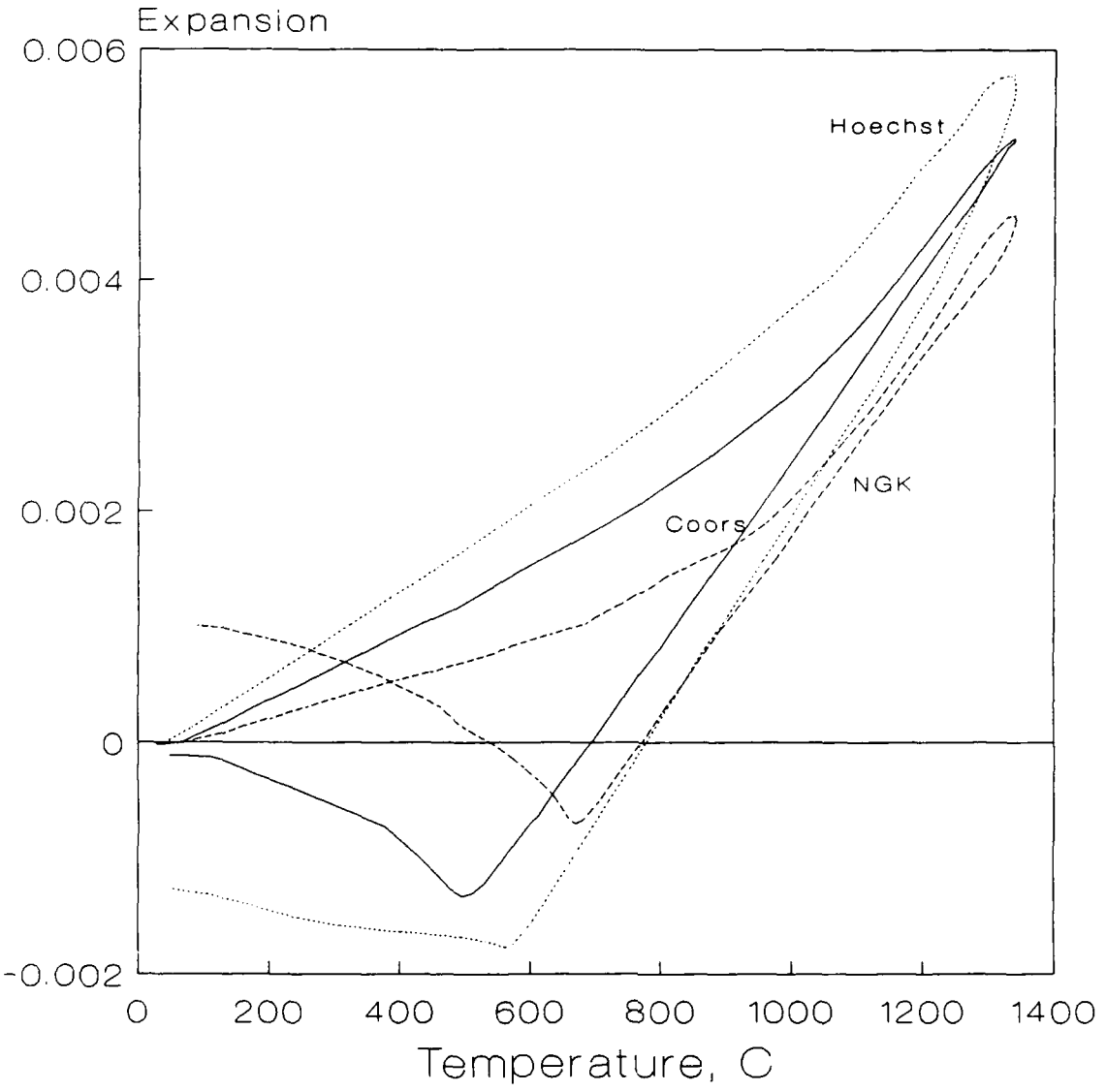

Figure 10: Cast Thermal Expansion Curves

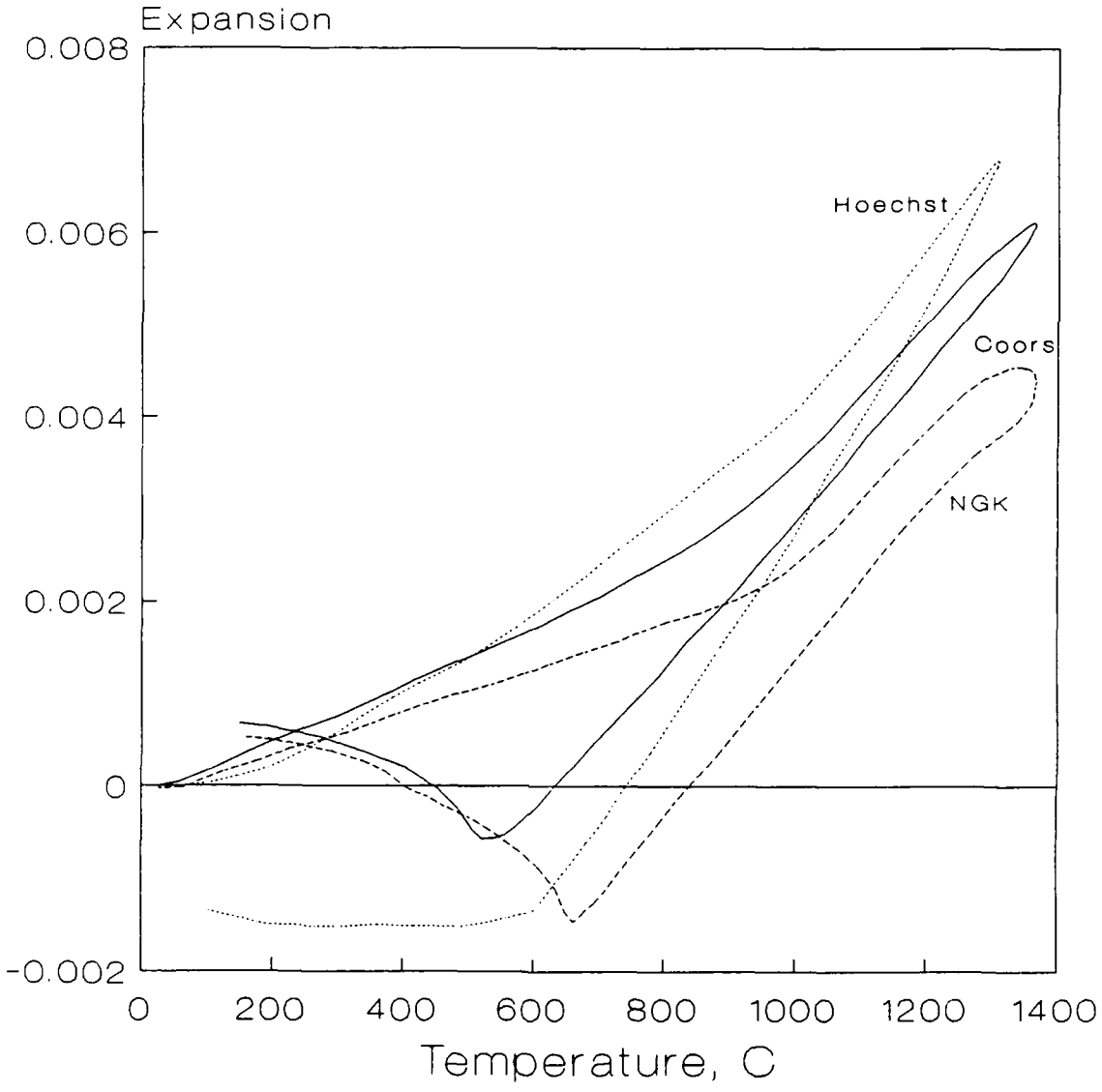

Figure 11: Cast Iron Thermal Expansion

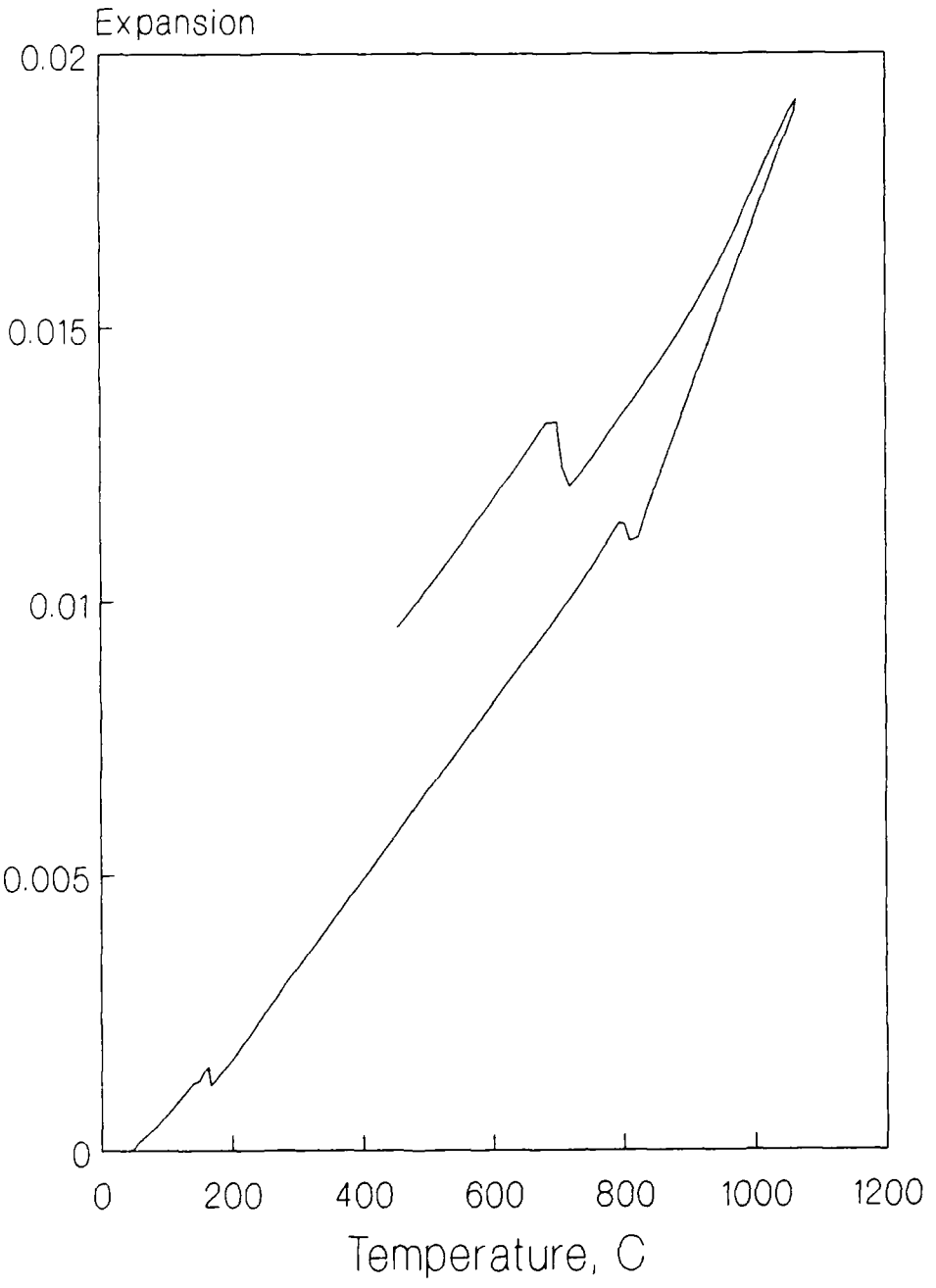

Figure 12: As-Received Thermal Conductivity

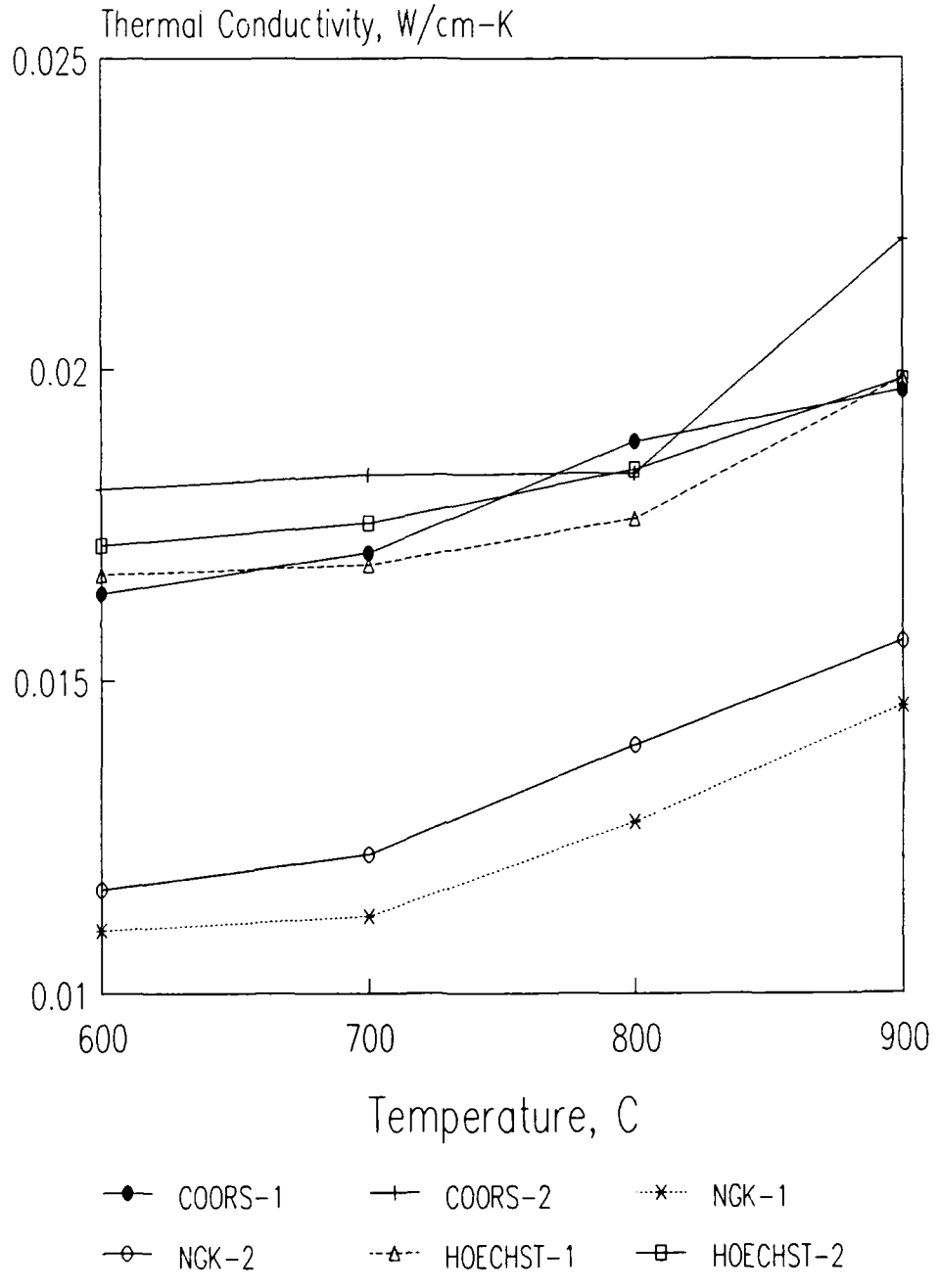

Figure 13: Cast Iron Thermal Conductivity

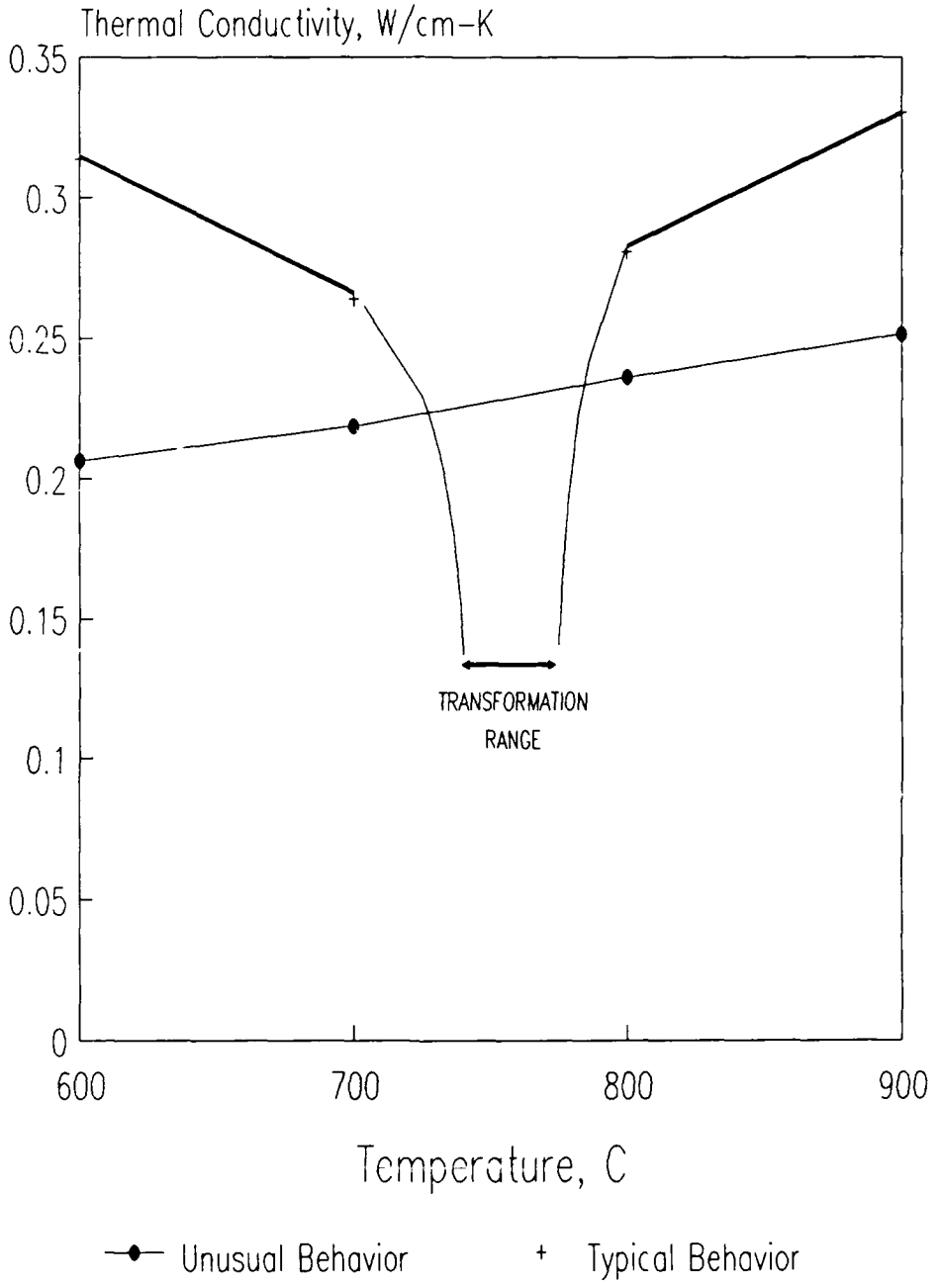

PHASE II: ENVIRONMENTAL EXPOSURE

Thermal/Oxidation Studies

Flexural Strength

Flexural strength tests, on specimens of each of the aluminum titanates were conducted after the thermal exposures. Table 4 and Figures 14 (Lot A) and 15 (Lot B) show the data for each simulated exhaust temperature after the two simulated casting condition exposures.

The Coors material did not exhibit any loss in strength after exposure to the different simulated exhaust temperatures for either the Lot A or Lot B samples. There was no appearent difference in strength between Lot A and Lot B.

The Hoechst material did not show any loss in strength after exposure to simulated exhaust temperatures #1, #2 and #3 for either Lot A or Lot B sample. The Lot B sample showed a decrease in strength compared to the Lot A samples. The small number of specimens tested does not allow any conclusions to be drawn as to whether there is a true difference in strength. Additional samples need to be tested to make this determination.

After simulated exhaust temperature exposure #4, the Hoechst material showed a great increase in strength (650 to 800%) for the Lot A and Lot B sample. This drastic change in the material properties indicates that the exposure has induced a change in the material structure.

The NGK material did not show any loss in strength after exposure to the different simulated exhaust temperature exposures when compared to the Lot A and Lot B baseline samples. The material showed a decrease in strength for the Lot B sample similar to that seen for the Hoechst material, but again, additional samples need to be tested to determine if the difference is significant. There is no data reported for the NGK material after the 815/500 exposure in the Lot A sample, because all specimens were broken during handling prior to testing. It is unlikely that this is due to the thermal exposure, but is due to the inherent weakness of the NGK material.

Fractography

The fracture surfaces of the flexural test samples were examined under an optical microscope. As was encountered with the as-received samples, the low strength and microstructural porosity did not allow determination of fracture origins.

Table 4: Flexural Strength After Exposure

Material		Flexural Strength, MPa			
		Baseline	540°C/500 h	815°C/500 h	1090°C/500 h
Lot A					
Coors	Mean	31.30	37.33	37.33	35.22
	Std Dev	4.11	1.93	1.93	0.0
	n	9	5	5	4
Hoechst	Mean	22.45	25.36	22.01	123.26
	Std Dev	2.62	3.86	1.76	9.96
	n	8	5	4	5
NGK	Mean	9.39	11.45	--	14.09
	Std Dev	1.76	1.76	--	0.0
	n	9	4	--	4
Lot B					
Coors	Mean	32.05	32.40	37.86	42.96
	Std Dev	2.00	2.95	3.37	6.30
	n	10	5	4	5
Hoechst	Mean	10.21	11.97	16.90	122.55
	Std Dev	3.88	4.02	1.58	7.22
	n	10	5	5	5
NGK	Mean	7.04	7.04	10.57	7.04
	Std Dev	0.0	0.0	0.0	0.0
	n	9	2	4	2

Microstructure

The microstructures of the aluminum titanates after the different simulated exhaust temperature exposures were similar to the furnace exposure microstructures in Figure 3, except for the Hoechst material after simulated exhaust temperature exposure #4 in both the Lot A and Lot B sample.

These microstructures showed an increased white phase and finer grain structure than was seen in the furnace exposure and simulated exhaust temperature exposures #1, #2 and #3. The microstructure of the Lot A, simulated exhaust temperature exposure #1 and #4 samples are compared in Figure 16.

Figure 14: Lot A Flexural Strength

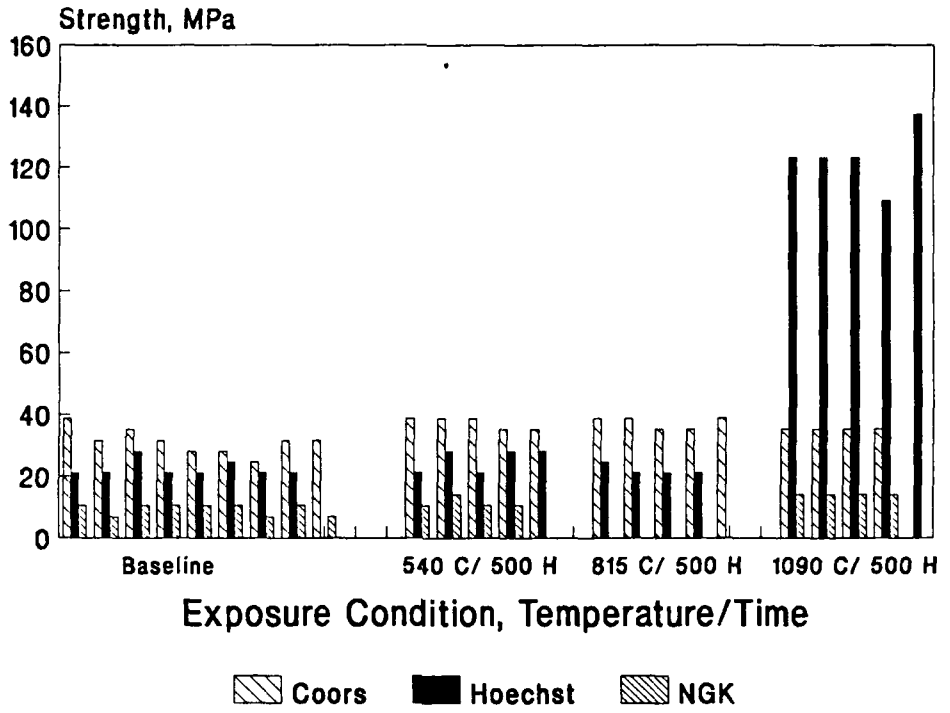

Figure 15: Lot B Flexural Strength

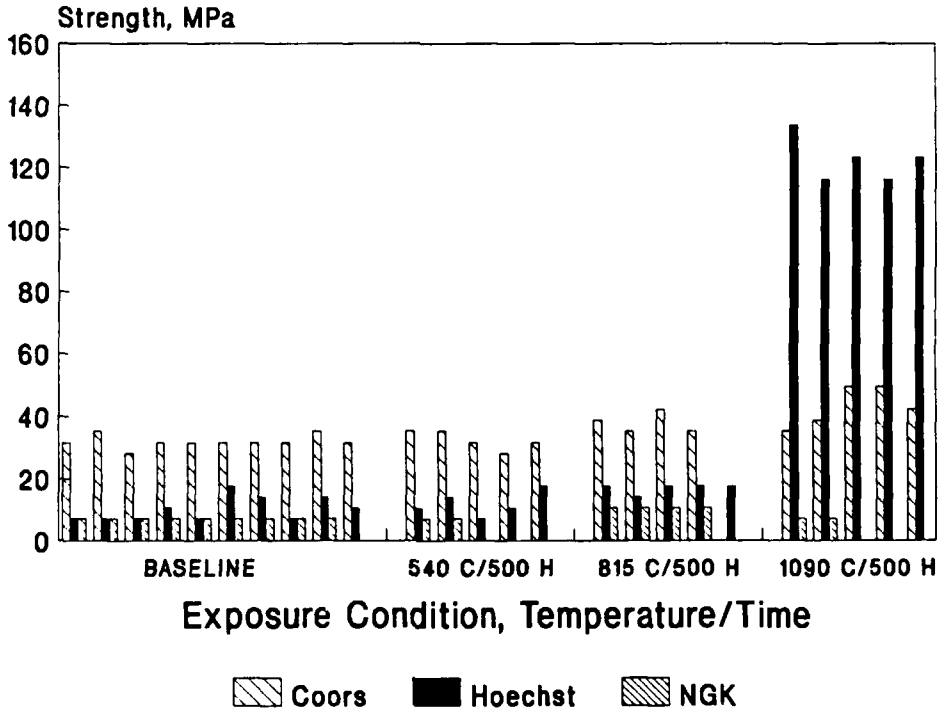

Figure 16: Hoechst Simulated Exhaust Temperature Exposure #1 and #4 Microstructures

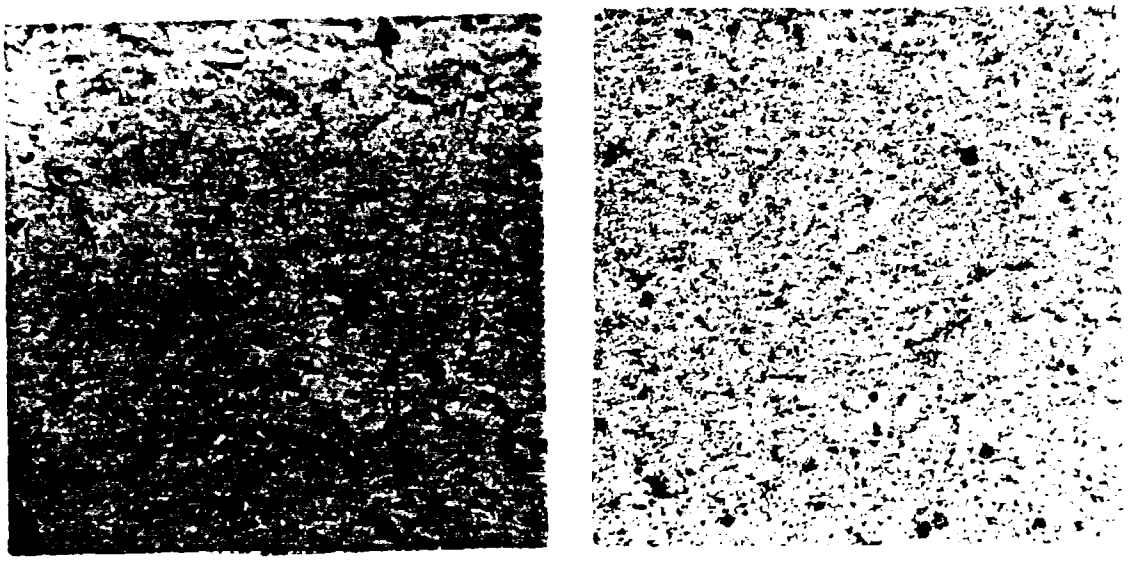

Exposure Condition #1
100X

Exposure Condition #4
100X

Elemental and Phase Composition

The overall elemental composition of the samples after each of the simulated exhaust temperature exposures were determined by SEM Energy Dispersive Analysis. The compositions for each of the materials were consistent with the cast compositions in Table 3.

X-Ray Analysis

The crystal structure of the Hoechst material after simulated exhaust temperature exposure #4 was examined using x-ray diffraction. The diffraction pattern for this sample was distinctly different from the as-received or cast x-ray diffraction patterns. The x-ray diffraction pattern of the Lot A, simulated exhaust temperature exposure #4 sample is shown in Figure 17. The phases identified from the pattern were Al_2TiO_5, α-Al_2O_3, and a Ti-Fe-Mg-Al composite oxide.

Thermal Expansion

The thermal expansion curves for each of the NGK and Coors samples, after the different simulated exhaust temperature exposures, showed the same shape as the cast thermal expansion curves (Figure 10). As the simulated exhaust exposure temperature increases, the final length for samples of both materials changes

from a net increase (simulated exhaust temperature exposure #1) to a net decrease (simulated exhaust temperature exposures #3 and #4).

The thermal expansion curves for the Hoechst material after simulated exhaust temperature exposures #1, #2 and #3 showed no differences from the cast thermal expansion curve. However, the thermal expansion curve for the material after simulated exhaust temperature exposure #4, was significantly different. This curve was fairly linear and did not exhibit a hysteresis loop typical of the aluminum titanates. The curve closely resembled a thermal expansion curve of α-Al_2O_3.

Diesel Exhaust Exposure

Engine induced vibration of the sample holder assembly in the exhaust ducting, combined with the low inherent strength of the materials, resulted in failure of the test specimens during exposure.

In discussions with Mr. Jeffery Swab of MTL, it was agreed that this data could not be collected because of the specimen failures during exhaust exposure.

Cylinder Head Casting

The ports with the ceramic foam compliant layer were the only ports to survive the casting intact. All other ports failed by spalling on the inner surface.

Since several of the ports survived casting, it was decided to investigate the behavior of the port in an engine test. One of the cylinders with a surviving port was chosen for machining to a single cylinder head.

The multi-cylinder head was cut and machined to a single cylinder configuration. Figure 18 shows a photograph of the finished single cylinder head. Imprecise placement of the ports in the core prior to casting resulted in several problems during machining of the single cylinder head, including one operation where the machining tool touched the port and produced some damage. Since the objective was to examine the behavior during an engine test for proof-of-concept, the port was repaired with a ceramic high temperature adhesive.

This head survived the single cylinder engine test for several hours with no additional damage to the ceramic demonstrating the potential success of the cast-in-place concept for insulated heads.

Figure 17: Hoechst Simulated Exhaust Temperature Exposure #4
X-Ray Diffraction Pattern

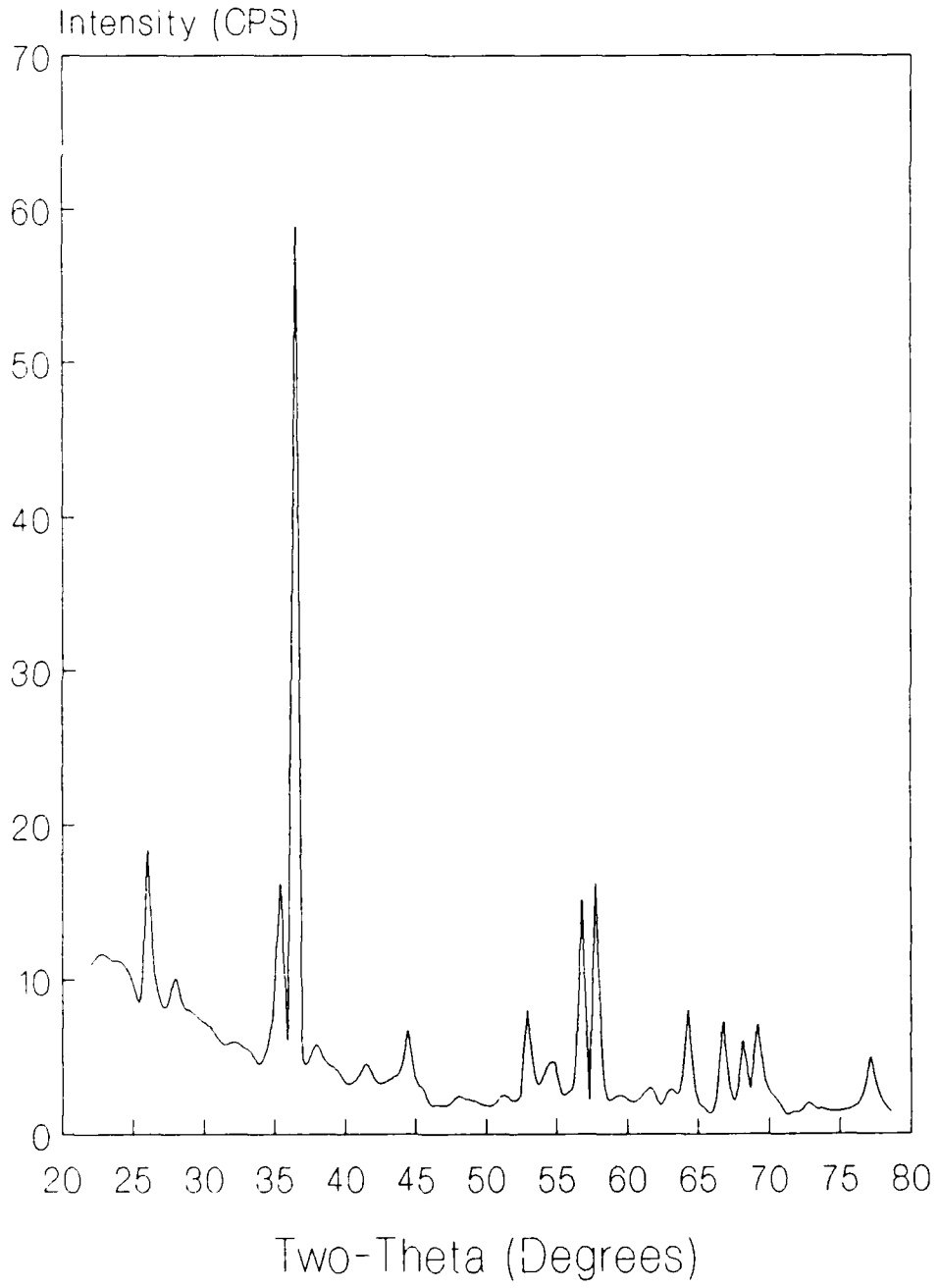

Figure 18: Ceramic Port in V-903 Engine Head

PHASE III: INSTRUMENTED CASTING TRIALS

Cummins investigated the feasibility of the cast-in-place ceramic port concept in conjunction with foundry technologists at Golden Foundry and Case Western University. Most of the effort was conducted through trial and error processes. Instrumented casting trials will supply necessary information for future modelling studies as well as information concerning the actual casting process.

Preliminary Casting Studies

The initial casting studies were undertaken to investigate some of the casting parameters which would affect the survival of the cast-in-place port.

Figure 19 shows a diagram of the thermocouple locations to instrument the sample ports for the final casting trials. These locations were determined by thermocouple survival and performance in the preliminary casting work.

The parameters to be investigated in the final casting will involve instrumentation and testing of ports with two different compliant layers in combination with four different core sand materials. Core sands to be tested include silica (SiO_2), zircon ($ZrSiO_4$), SiC and SiC with iron shot in the matrix.

Figure 19: Thermocouple Locations for Instrumented Casting

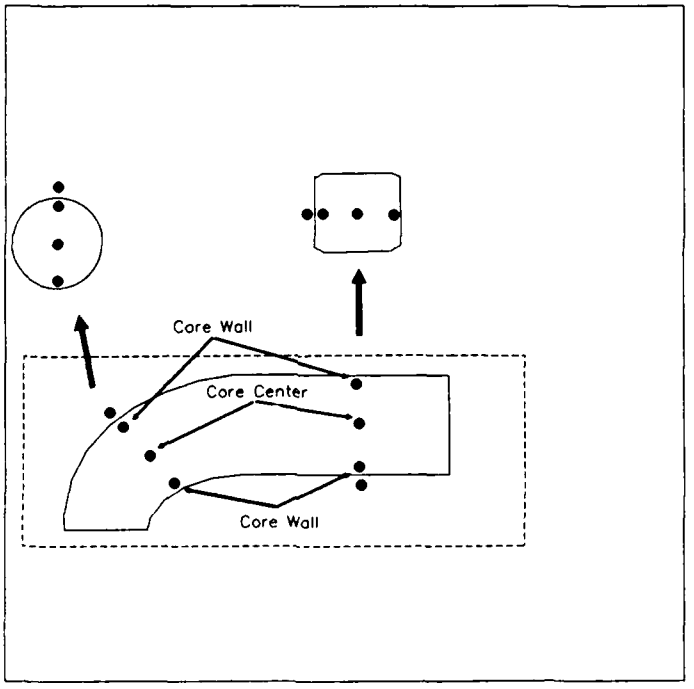

Final Casting Studies

Figure 20 shows the temperature profiles with respect to time at the center core location of the port for the four runs containing a paper layer on the port. The most significant phenomena to note is the presence of a temperature/time lag at approximately 100°C for each core sand composition. This phenomena represents the evaporation of water from the core sand. The more thermally conductive sands (SiC & SiC/Fe) heat up and cool faster than the lower conductive sands. As expected, SiO_2 sand requires a longer time to heat up in the core center and subsequently, retains that heat for a longer time than the other sands. The pattern for the $ZrSiO_4$ sand is much different than any of the other sands. The profile for the $ZrSiO_4$ is not fully understood at this time.

Figure 21 shows similar data for each core sand composition at the core wall location of each casting containing no compliant layer. There is no apparent lag in initial heat-up of the core sand at the wall location, due to the proximity of the core wall to the surrounding metal being poured. This data reveals that the SiC/Fe sand has a more pronounced cooling effect, especially around 700°C, due to its higher thermal conductivity. This cooling may occur because of the transformation in iron at this temperature.

Figure 22 shows the gradient that exists from core wall to core center during cooldown of the casting. It is interesting to note the significant reduction in the thermal gradient from core wall to core center for the SiC/Fe core composition due to its higher thermal conductivity. A core sand with a higher thermal conductivity exhibits an even distribution of heat from port to the center core which should result in fewer failures in the port during casting.

Core Sand Considerations

Thermal expansion studies were conducted on the core sands used in the final casting studies above.

Figure 23 shows the thermal expansion profiles for the SiO_2, $ZrSiO_4$, SiC and 50% SiC/50% Fe core sands respectively. Each thermal expansion curve represents the material's expansion behavior over the range 25 to 900°C.

The three ceramic sands (i.e. SiO_2, $ZrSiO_4$, SiC), show a tremendous contraction above 500°C on cooling, which results in an overall decrease in length. The 50% SiC/50% Fe sand, on the other hand, does not exhibit the contraction and this sand shows a permanent length increase upon cooling to room temperature.

Figure 24 shows photographs of the castings in which no compliant layer was used for the SiO_2, $ZrSiO_4$, SiC and 50% SiC/50% Fe core sand compositions, respectively. The casting in which the SiC/Fe sand was used reveals no evidence of damage to the ceramic.

Figure 20: Time/Temperature Profiles: Center Core

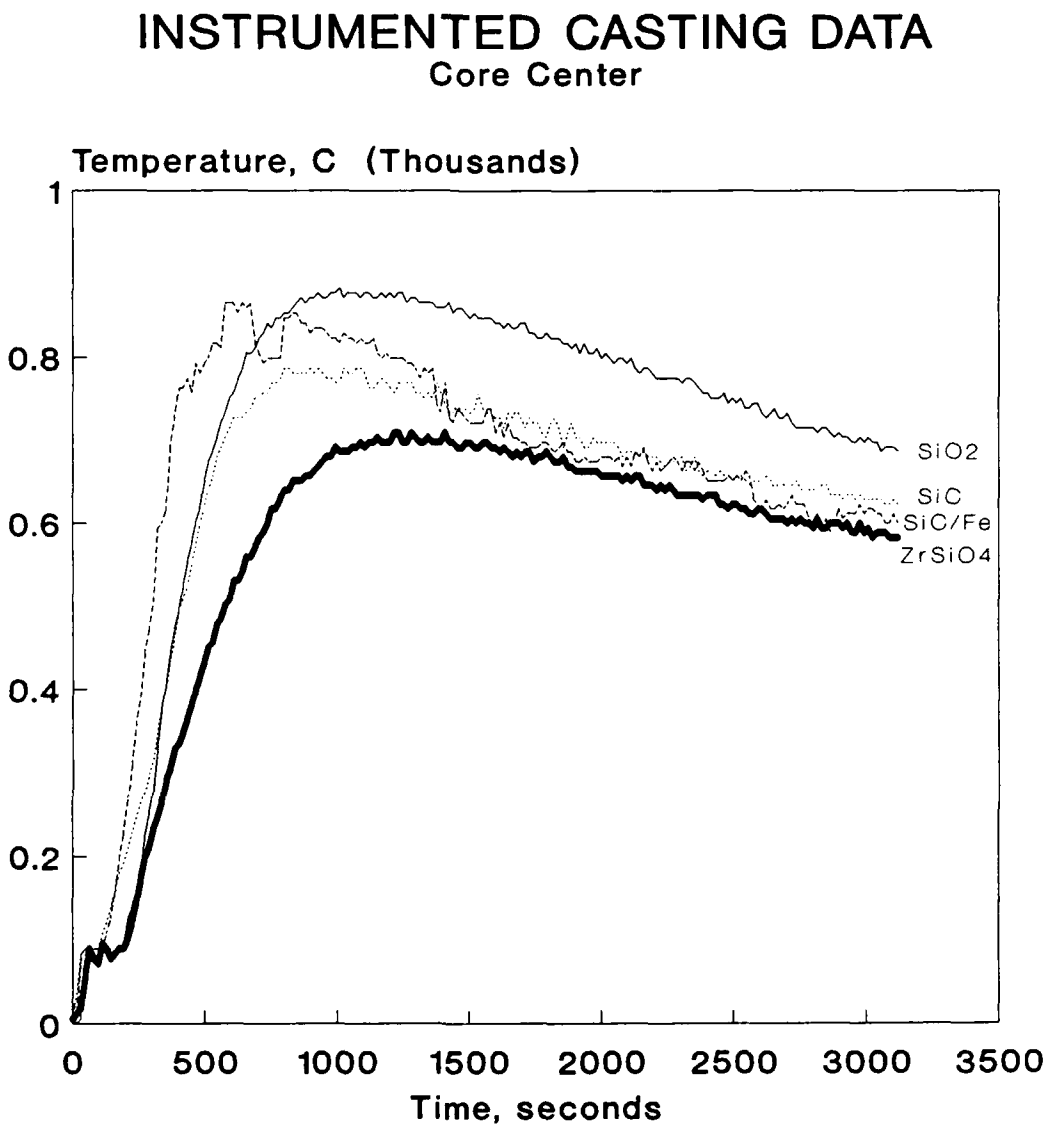

Figure 21: Time/Temperature Profiles Port Wall

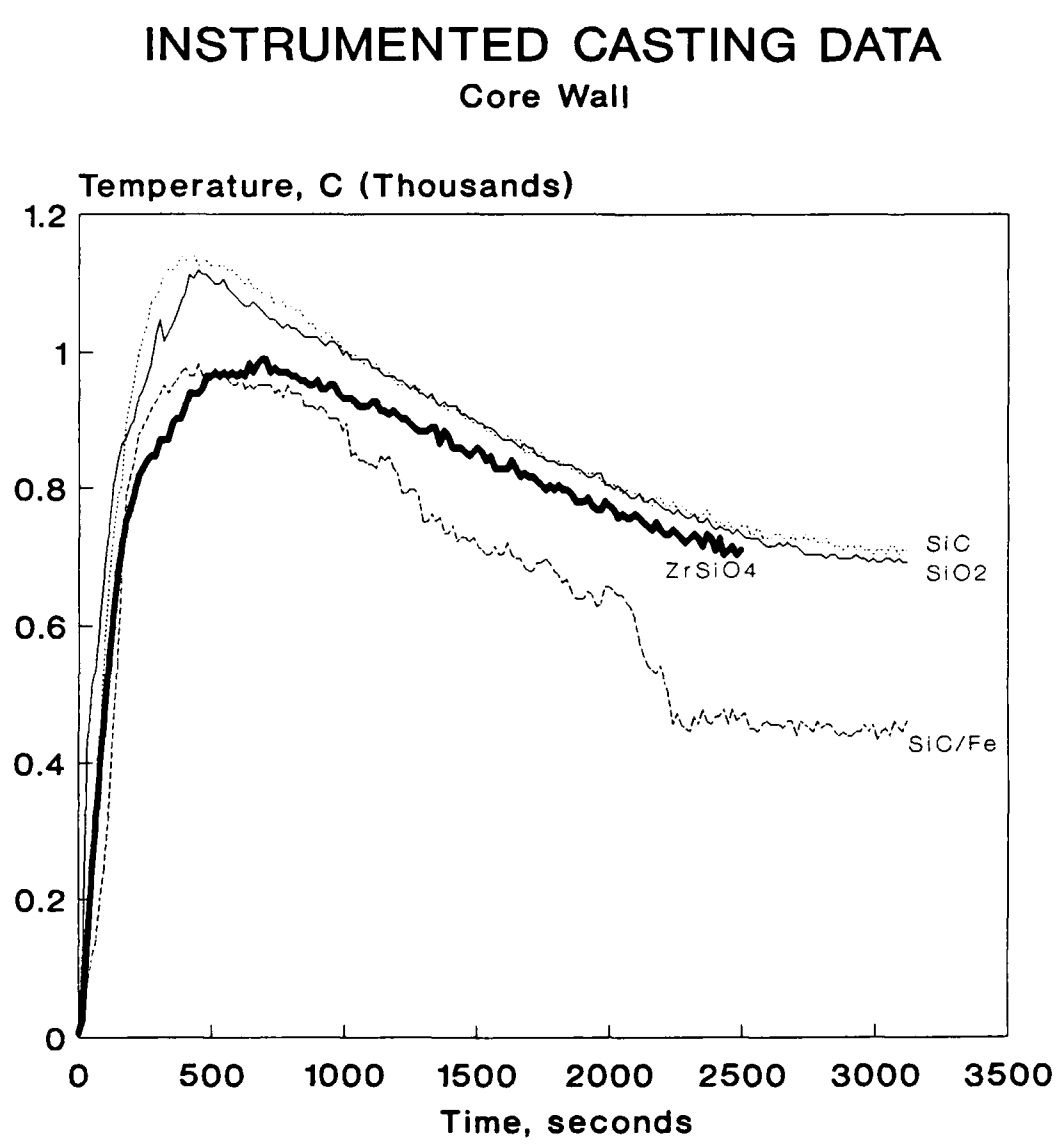

Figure 22: Port Wall to Core Center Thermal Gradient

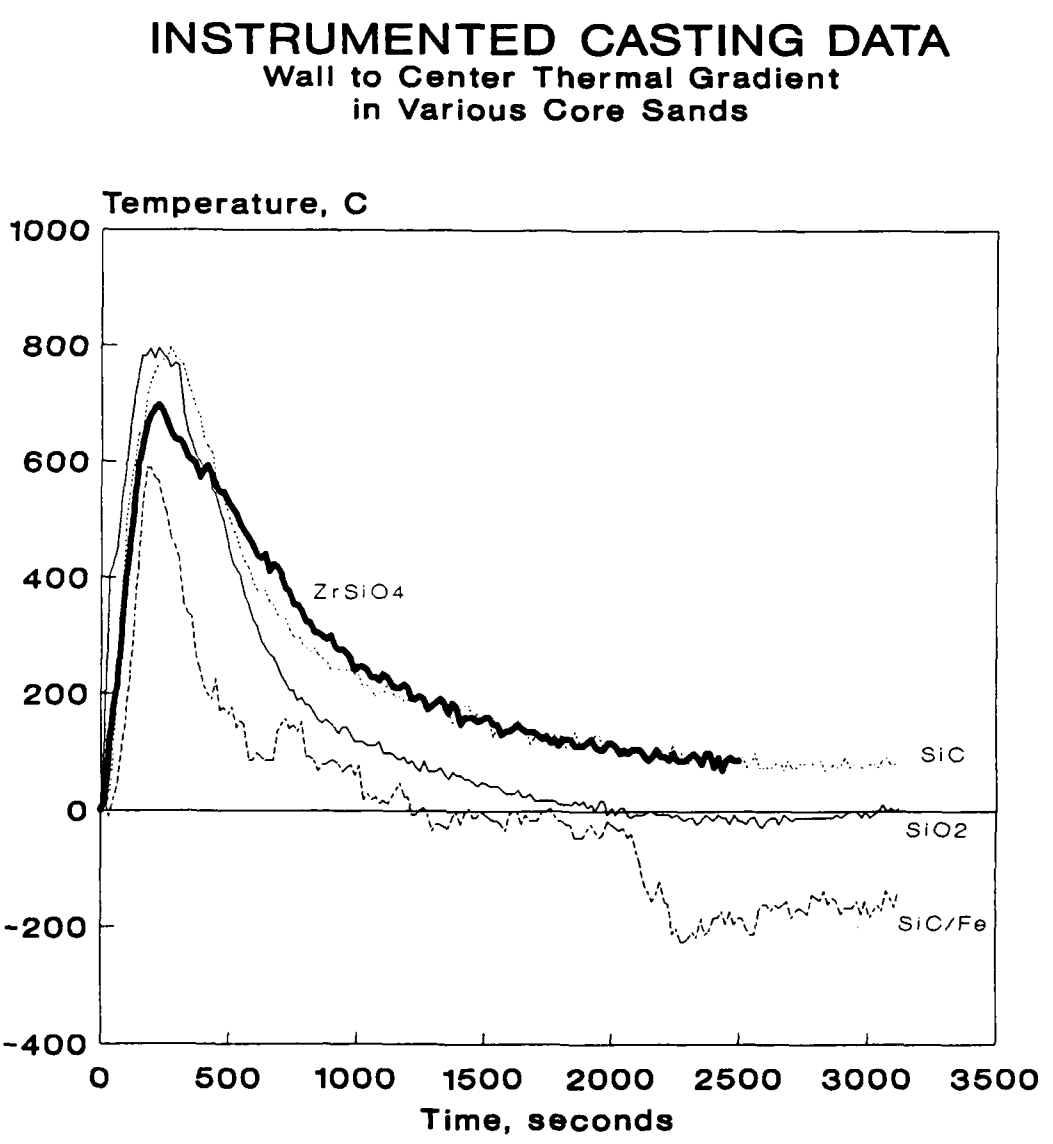

Figure 23: Core Sand Thermal Expansion

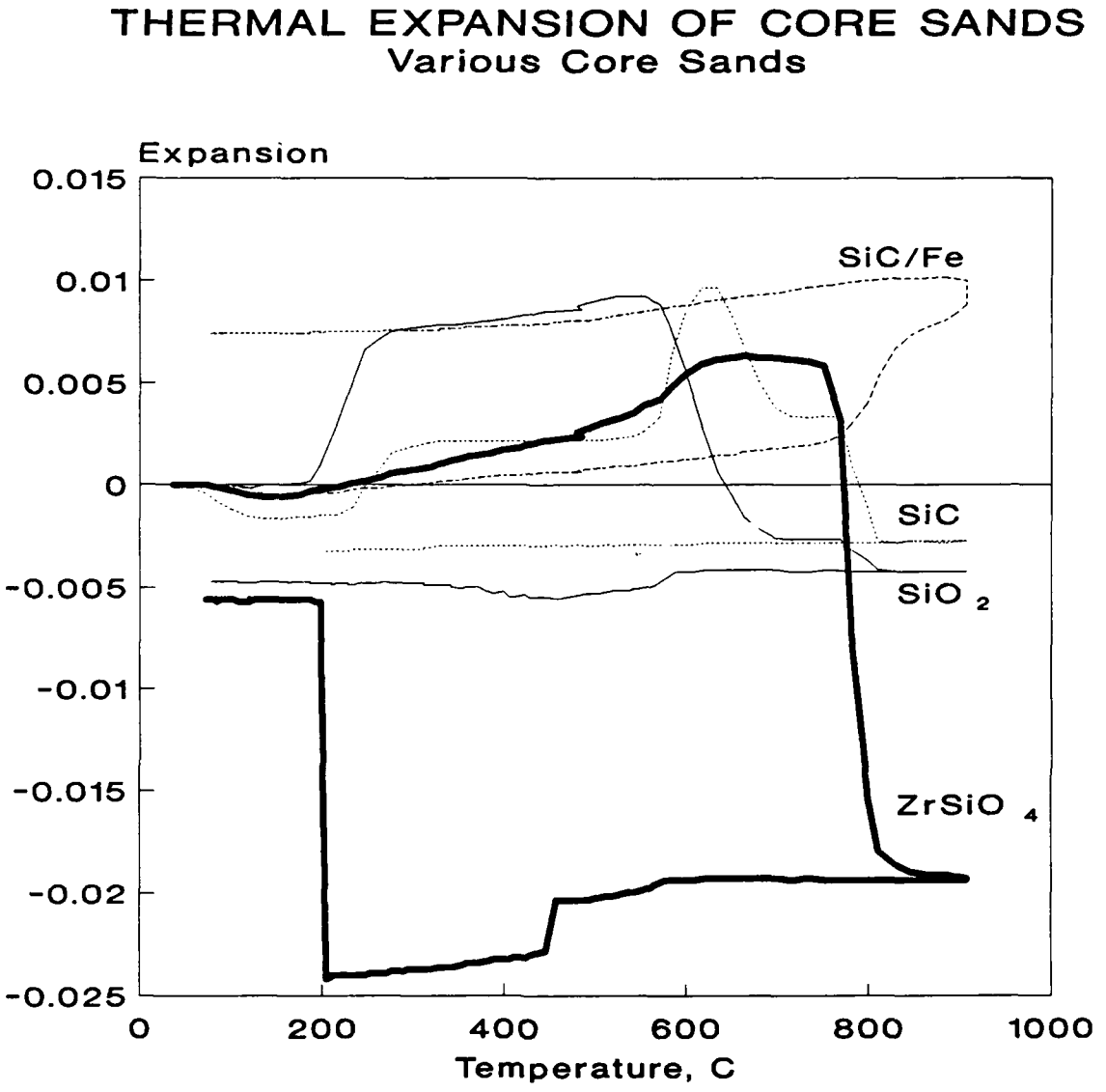

Figure 24: Core Sand Effects on Single Port Castings with No Compliant Layer on the Port

SiO_2 Core Sand

$ZrSiO_4$ Core Sand

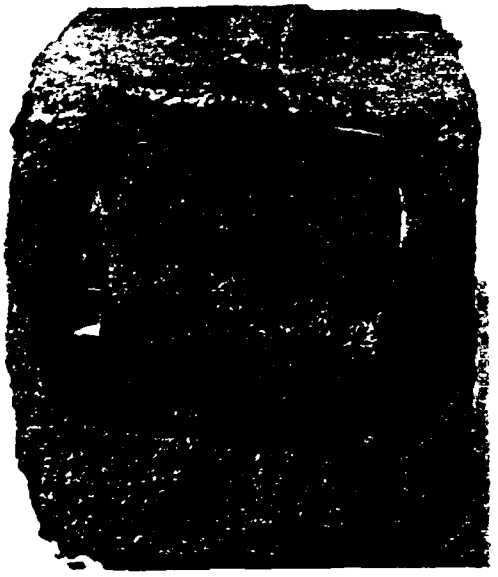

SiC Core Sand

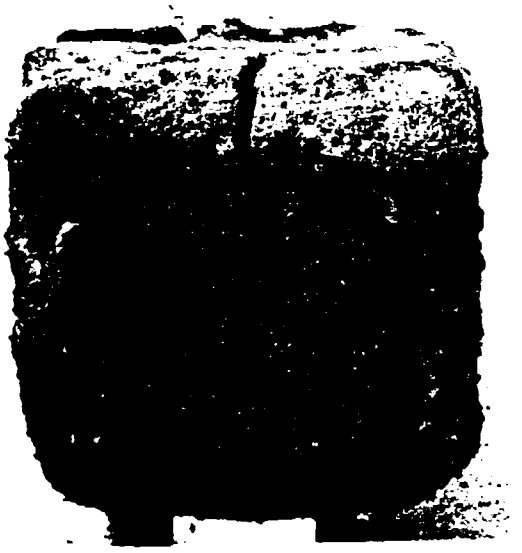

SiC/Fe Core Sand

DISCUSSION:

Aluminum titanate is a material that shows promise as a cast-in-place intake and exhaust ports. The material has very interesting thermal properties, but lacks the strength and toughness of many advanced ceramics.

The physical and mechanical properties of the aluminum titanates from different suppliers vary greatly. This has been shown in some earlier work at Cummins [11,12,13] and correlates with the current work.

The relationships between grain size, microcracking and mechanical properties have been reviewed by Thomas and Stevens.[5] More recent work by Parker and Rice [6] correlates the grain size and microcracking with thermal expansion and strength. This work showed that there is a critical grain size for microcrack formation. When the grain size exceeds the critical value, microcracks form at the grain boundaries. The extent of microcracking affects the measured properties for the material.

Aluminum titanate from NGK is low density with an extensive crack structure and has low strength, low modulus and low thermal conductivity. The Coors and Hoechst aluminum titanates were higher density and had a similar thermal conductivity. The Coors material had a fine grained structure and the Hoechst material had a coarse grained structure with very little cracking in either material. The fine grained Coors material had higher strength and modulus than the coarse grained Hoechst material.

The NGK material was severely microcracked as shown by the low thermal conductivity, low strength and modulus values. The thermal expansion curves were typical of a microcracked structure with a hysteresis loop occurring over a heating and cooling cycle. The hysteresis comes from the anisotropic expansion (expansion along a and b axes and contraction along c axis) of the grains with microcrack healing occurring during heating, then direct contraction without microcrack formation on cooling until a critical temperature (around 500 to 700°C) is reached and the final stage of grain contraction with microcrack formation causing growth in the material.

The aluminum titanate from Coors was a dense material with some microcracking as shown by the thermal expansion behavior. The relatively high values for thermal conductivity, strength and modulus indicate that the microcracking was not extensive. Exposure to temperature appeared to cause consolidation and grain growth with resultant drop in strength. This behavior was predicted by the work of Parker and Rice.[6] The retention of an Al_2TiO_5 phase structure after all exposures indicates that the additives are effective in stabilizing the structure.

The aluminum titanate from Hoechst also was a dense material with some microcracking. The thermal expansion curves showed the characteristic hysteresis loop. The Hoechst material had a larger grain size than the Coors material and had lower strength and modulus. The thermal conductivity was in the same range as the Coors material indicating that the extent of microcracking was similar. During the thermal degradation exposure (5 h at 980°C), the Al_2TiO_5 showed decomposition and growth of a free TiO_2 phase, indicating that the phase stabilization additives were not effective at high temperatures (above 950°C). This result was confirmed by the flexural strength, thermal expansion and phase structure results after 500 h exposure at

1090°C. The flexural strength increased 550%, the thermal expansion curve was linear with no hysteresis and the phase structure was representative of α-Al_2O_3.

Casting aluminum titanate in iron was a significant challenge. In the initial cooling of the casting, the cast iron contracts very rapidly against the weaker aluminum titanate, which cannot contract as fast. Shortly after the cast iron cools through the transformation range at 720°C, it contracts very rapidly and the aluminum titanate begins to expand significantly. It is possible that this temperature during cooldown is the most critical in the casting operation, since the weaker ceramic must withstand the compressive forces of the cast iron while expanding directly against it.

The behavior of the core sands has several implications in terms of the casting of ceramic exhaust ports into cast iron heads. Considering the behavior of the core sands during the cooldown stage of the casting process, it is evident that the SiO_2 and $ZrSiO_4$ sands, and to a lesser extent, the SiC sand lose the ability to support the ceramic port during the critical stages of cooling because of the length contraction of the cores. However, the 50% SiC/50% Fe sand gives greater support to the ceramic during cooldown with the possible result of reduced failures in the ceramic.

SiC and SiC/Fe core sand combinations resulted in castings of significant promise. Optimization of core sand compositions coupled with research into design, analysis and compliant layer technology appear to be necessary avenues to achieving success in casting ceramic port materials in gray iron.

The casting in which the SiC/Fe sand was used reveals no evidence of damage to the ceramic. This is quite impressive since there was no compliant layer in place to help increase the probability of survival of the ceramic. However, hot tearing of the metal is evident, which suggests the necessity of optimizing the expansion behavior of the 50% SiC/50% Fe sand by varying the concentration of the iron.

Figure 25 shows the expansion curves of Al_2TiO_5, the SiC/Fe sand and gray cast iron. The profile for the 50% SiC/50% Fe sand is very similar to the profile for gray cast iron in terms of the expansion behavior of the material. In both cases, we see a high degree of increase in expansion at approximately 700°C because of the transformation typical in cast iron. However, the presence of the SiC in the material maintains the overall expansion lower than that typical of cast iron. Reducing the composition of the iron in the core sand may help bring the core sand expansion closer to that of the gray cast iron during the critical cooldown stage (i.e. below 400°C) and result in a higher degree of integrity in the metal itself.

The use of different compliant layers was investigated in terms of the integrity of the finished casting. Previous casting studies [13,14,15,16] have revealed that the use of compliant layers results in improved integrity of the finished casting. The effect of the compliant layers, on the integrity of the casting, could not be differentiated from the effect of the different core sand in this study.

Figure 25: Thermal Expansion Comparison of Casting Materials

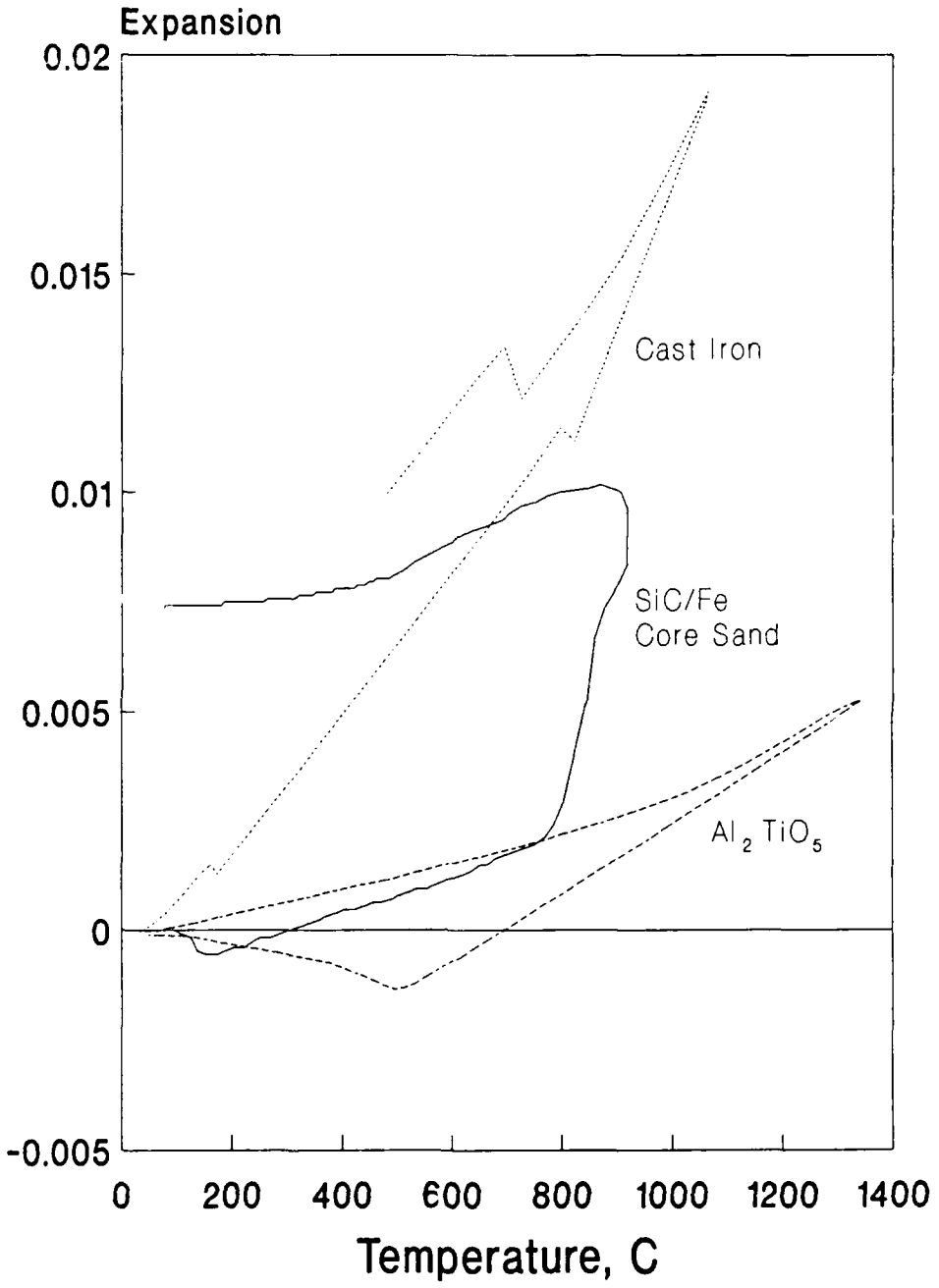

CONCLUSIONS:

Aluminum titanate is a relatively weak ceramic material with excellent thermal shock resistance, unusual thermal expansion characteristics, and a low thermal conductivity which permits it to be used as cast in place insulation.

The material evaluation carried out in this study shows that there are significant differences in the strength, stability and thermophysical properties of aluminum titanates from different suppliers. This variation in the material is another variable which must be taken into consideration when producing a finished component.

The casting procedures developed in this work have shown that a port of aluminum titanate material can be successfully incorporated into an iron casting, but additional work is necessary to tailor the casting process parameters and reduce the failure rates for the ceramic port.

Incorporation of an insulating aluminum titanate exhaust port into a state-of-the-art diesel engine head remains a significant challenge. The development of a cylinder head with insulating ports will require major changes to the cylinder head, port design, exhaust port material, and the casting procedure. These efforts will require major time and financial commitments to be successful for diesel applications.

RECOMMENDATIONS:

1) The mechanical properties of aluminum titanate need further development to produce a more robust ceramic component resulting in a higher probability of survival during casting.

2) Further casting work should be performed to analyze the casting parameters of importance and optimize the casting process.

3) Design & analysis of the cast-in-place system, using modelling and information developed in additional instrumented casting studies, is necessary to characterize the important design criteria in the casting process.

ACKNOWLEDGEMENTS:

The authors are grateful for the assistance of Mr. Terry Underwood and Mr. Mark Fear in conducting the experimental work at Cummins and Dr. J. F. Wallace for his assistance and gracious use of the casting facilities at Case Western Reserve University. We also thank Dr. R. E. Taylor, Mr. H. Groot and Mr. J. Larimore at the Thermophysical Properties Research Laboratory and Mr. Bill Simpson and Dr. Ray Johnson at Oak Ridge National Laboratory for their input and experimental work.

Mr. John Cogburn is presently employed at SELEE Corp. in Hendersonville, NC.

REFERENCES:

[1] J.H. Rush, "Exhaust Port Heat Rejection in a Piston Engine: A Preliminary Report," Society of Automotive Engineers (SAE) Paper No. 760766, (1976).

[2] S.D. Hires and G.L. Pochmara, "An Analytical Study of Exhaust Gas Heat Loss in a Piston Engine Exhaust Port," SAE Paper No. 760767, (1976).

[3] J.F. Tovell, "The Reduction of Heat Losses to the Diesel Engine Cooling System," SAE Paper No. 830316, (1983).

[4] D.H. Reichenbach, "Analysis of Exhaust Port Heat Rejection on the LHR-600 V903 Engine," Cummins Engine Co. (1986).

[5] H.A.J. Thomas and R. Stevens, "Aluminium Titanate - A Literature Review, Part 1: Microcracking Phenomena," Br. Ceram. Trans. J., **88**, 144-151 (1989).

[6] F.J. Parker and R.W. Rice, "Correlation between Grain Size and Thermal Expansion for Aluminum Titanate Materials," J. Am. Ceram. Soc., **72** [12] 2364-66 (1989).

[7] D. Sherman, "The 944 Turbo Engine," Car and Driver, April 1985, 52-54.

[8] H. Korkemeier, "Baptism of Fire," Christophorus - Magazine for Porsche Friends, **208**, 26-28 (1987).

[9] B. Miller, W. Coblenz and N Paille, Jr., "Development of a Ceramic Exhaust Port Liner, SAE Paper No. 880677, (1988).

[10] D.T.Y. Huang, D.K.S. Chen and D.L. Van Ostrom, "Finite Element Reliability Analysis of a Ceramic Exhaust Port Liner Subjected to Thermomechanical Interactions During Casting," SAE Paper No. 880678, (1988).

[11] J.W. Cogburn, "Thermophysical Properties of Thermal Insulation Materials," Cummins Engine Co. (1986).

[12] W.F. Mandler, "Analysis of Feldmuhle's Tialit Material," Cummins Engine Co. (1983).

[13] T.M. Yonushonis, T.L. Underwood, M.P. Fear, "Aluminum Titanate Port Materials - Interim Report," Cummins Engine Co. (1986).

[14] T.L. Scofield, "Casting of Ceramic Exhaust Ports into Cylinder Heads," Cummins Engine Co. (1983).

[15] T.M. Yonushonis and R.G. Weldon, "Aluminum Titanate Cast in Iron - Interim Report," Cummins Engine Co. (1987).

[16] T.M. Yonushonis and T.L. Underwood, "Insulating Aluminum Titanate Ports Cast in Iron," Cummins Engine Co. (1987).

APPENDICES:

APPENDIX
A

NDE MEASUREMENTS ON ALUMINUM TITANATE

Seven samples of aluminum titanate were obtained for ultrasonic elastic modulus determination. These samples consisted of two specimens each from Coors and Hoechst and three samples from NGK. The material included one as-received and one after-casting sample from each vendor and one additional small after-casting piece from NGK. Since the samples were quite porous, typical fluids could not be used to couple ultrasonic signals into the samples. Instead, a viscous material normally used to couple shear waves into elastic media was used to introduce both transverse and shear waves into the specimens. The elastic wave velocities were then measured at five points on each sample and the results averaged. As expected, there was considerable variation from point to point on each sample, particularly for the NGK samples. In fact, the point-to-point variation was greater for each sample than the difference in the averaged values of the as-received and after-casting samples for each vendor. For the NGK material, the variation in the elastic wave velocities between the two after-casting samples was greater than that between one of the after-casting samples and the as-received sample.

Since the density of each sample was required to compute the elastic moduli and since none of the samples was suitable for immersion density determination, a rough value was obtained from Cummins. The values communicated were 3.14 gm/cm^3 (Coors), 2.98 gm/cm^3 (NGK), and 3.23 gm/cm^3 (Hoechst). Using these values and the elastic wave velocities previously determined, estimates for the shear modulus, Poisson's ratio, and Young's modulus were calculated using the well-known linear elastic relations.[1] An error analysis of the data obtained on the NGK samples indicates than the r.m.s. error in the shear and Young's moduli is 10% and 17%, respectively, but is 224% in the value of Poisson's ratio. This is unavoidable because of the extreme variability in the samples. The statistical error in the Coors and Hoechst samples is somewhat less.

[1] Robert C. McMaster, *Nondestructive Testing Handbook II*, Ronald Press, New York, 1959.

SYMBOLS USED IN ELASTIC MODULUS DETERMINATION

V_l	Compressional wave velocity
V_t	Transverse (shear) wave velocity
rho (ρ)	Material density
mu (μ)	Shear Modulus (first Lamé constant)
lambda (λ)	Second Lamé constant
sigma (σ)	Poisson's ratio
Y	Young's modulus

The moduli are calculated using the measured wave velocities and the following relationships for linear, isotropic media:

$$V_t = \{\mu/\rho\}^{\frac{1}{2}} \quad ; \quad V_l = \{(\lambda + 2\mu)/\rho\}^{\frac{1}{2}} \quad ; \quad Y = 2\mu(1 + \sigma) \quad ; \quad \text{and}$$

$$\sigma = (1-2\gamma)/(2-2\gamma) \quad ;$$

where $\gamma = (V_t/V_l)^2$.

Sample: NGK-as rec.

Vl(km/sec)	Vt(km/sec)	Rho(gm/cm**3)
1.772	1.214	2.980

mu(n/m**2)	lamda(n/m**2)	Poisson's Ratio	Young's Modulus(n/m**2)
4.392E+09	5.733E+08	5.773E-02	9.291E+09

Error analysis on NGK
velocities: ±5%
M: ± 10%
λ: ± 22%
σ: ± 20%
Y: ± 10%

Sample: NGK-cast 1

Vl(km/sec)	Vt(km/sec)	Rho(gm/cm**3)
1.998	1.380	2.980

mu(n/m**2)	lamda(n/m**2)	Poisson's Ratio	Young's Modulus(n/m**2)
5.675E+09	5.459E+08	4.388E-02	1.185E+10

Sample: NGK-cast 2

Vl(km/sec)	Vt(km/sec)	Rho(gm/cm**3)
1.815	1.218	2.980

mu(n/m**2)	lamda(n/m**2)	Poisson's Ratio	Young's Modulus(n/m**2)
4.421E+09	9.750E+08	9.035E-02	9.641E+09

Sample: Hst-as rec.

Vl(km/sec)	Vt(km/sec)	Rho(gm/cm**3)
3.261	2.170	3.230

mu(n/m**2)	lamda(n/m**2)	Poisson's Ratio	Young's Modulus(n/m**2)

1.521E+10	3.929E+09	1.026E-01	3.354E+10

Sample: Hot-cast

Vl(km/sec)	Vt(km/sec)	Rho(gm/cm**3)
3.257	2.170	3.230

mu(n/m**2)	lamda(n/m**2)	Poisson's Ratio	Young's Modulus(n/m**2)
1.521E+10	3.845E+09	1.009E-01	3.349E+10

Sample: Coors-as rec

Vl(km/sec)	Vt(km/sec)	Rho(gm/cm**3)
4.032	2.554	3.140

mu(n/m**2)	lamda(n/m**2)	Poisson's Ratio	Young's Modulus(n/m**2)
2.048E+10	1.008E+10	1.649E-01	4.772E+10

Sample: Coors-cast

Vl(km/sec)	Vt(km/sec)	Rho(gm/cm**3)
4.150	2.601	3.140

mu(n/m**2)	lamda(n/m**2)	Poisson's Ratio	Young's Modulus(n/m**2)
2.124E+10	1.159E+10	1.765E-01	4.999E+10

APPENDIX
B

PRL 775

Thermophysical Properties of Selected Materials

A Report to Cummins Engine Company, Inc.

by

R.E. Taylor, H. Groot and J. Larimore

March 1988

Properties Research Laboratory
Post Office Box 2224
West Lafayette, IN 47906

TABLE OF CONTENTS

LIST OF TABLES

LIST OF FIGURES

Thermophysical Properties of Selected Materials

INTRODUCTION

Samples of certain materials were submitted for thermal conductivity determinations. The samples are identified in Table 1. Thermal diffusivity (α) values were obtained using the laser flash technique. Bulk density (d) values were calculated from the diffusivity sample's geometries and mass. Specific heat (Cp) values were obtained using differential scanning calorimetry and thermal conductivity (λ) was calculated as a product of these quantities, i.e. $\lambda = \alpha \, Cp d$.

Specific heat was measured using a standard Perkin-Elmer Model DSC-2 Differential Scanning Calorimeter (Figure 1) using sapphire as a reference material. The standard and sample, both encapsulated in pans, were subjected to the same heat flux and the differential power required to heat the sample at the same rate was recorded using the digital data acquisition system (Figure 2). From the mass of the sapphire standard, pans, the differential power, and the known specific heat of sapphire, the specific heat of the sample is computed. The experimental data is visually displayed as the experiment progresses. All measured quantities are directly traceable to NBS standards.

Thermal diffusivity was determined using the laser flash diffusivity method. The flash method, in which the front face of a small disc-shaped sample is subjected to a short laser burst and the resulting rear face temperature rise is recorded, is used in over 80% of the present thermal dif-

fusivity measurements throughout the world. A highly developed apparatus exists at PRL (Figure 3) and we have been involved in an extensive program to evaluate the technique and broaden its uses. The apparatus consists of a Korad K2 laser, a high vacuum system including a bell jar with windows for viewing the sample, a tantalum tube heater surrounding a sample holding assembly, a spring-loaded thermocouple or an i.r. detector, appropriate biasing circuits, amplifiers, A-D converters, crystal clocks and a minicomputer based digital data acquisition system (Figure 2) capable of accurately taking data in the 40 microsecond and longer time domain. The computer controls the experiment, collects the data, calculates the results and compares the raw data with the theoretical model.

RESULTS AND DISCUSSION

Sample dimensions, masses and bulk density values are listed in Table 2. The density values sister samples are in close agreement.

Specific heat results are given in Tables 3 (Al_2TiO_5 samples) and 4 (cast iron and ZrO_2 samples), and are plotted in Figures 4 and 5. The specific heat of the Al_2TiO_5 samples all lie within a ±2% band and the extrapolation to higher temperatures presented no difficulties. The results for the other samples also fall within a relatively narrow band despite the differences in compositions. However, the extrapolation for the iron samples was not straight forward due to the Curie transformation near 780C.

Thermal diffusivity results are given in Table 5. The diffusivity results for the Al_2TiO_5 materials are plotted in Figure 6. The results for the NGK samples are lower than those for the other two materials in line with their lower density values. Thermal diffusivity values for the cast iron samples are plotted in Figure 7. These results are not in good agreement, especially at lower temperatures. The values for JWC-8 are similar to that of regular iron, whereas the values for JWC-7 are similar to an alloy. Diffusivity values for the TMY samples are plotted in Figure 8. The Zr_2C_3 sample has the lowest diffusivity and the sample with the most metal has the highest diffusivity.

Thermal conductivity results are calculated in Table 6. The conductivity values for the Al_2TiO_5 samples are plotted in Figure 9. The NGK samples have the lower conductivity values. The results for the Coors and Hoecsht materials are similar to each other. The conductivity values for the cast iron are plotted in Figure 10. The values for JWC-7 are significantly lower than those for JWC-8 and the temperature dependencies are also markedly different. The conductivity values of the TMY samples are plotted in Figure 11. The results for TMY-3 and -4 are almost identical despite their compositional differences. The results for TMY-1 are about half those for TMY-3 and -4.

Table 1

Sample Characterizations

Sample Identification	Description	
JWC-1	Coors Al_2TiO_5	
JWC-2	Coors Al_2TiO_5	
JWC-3	NGK Al_2TiO_5	
JWC-4	Hoecsht Al_2TiO_5	
JWC-5	Hoecsht Al_2TiO_5	
JWC-6	NGK Al_2TiO_5	
JWC-7	Cast Iron	
JWC-8	Cast Iron	
TMY-1	RM7P202-7-5	UTRC 88 to 92% ZrO_2
TMY-2	RM7P40/60	UTRC 40/60 ZrO_2/CoCrAlY
TMY-3	RM7P85/15	UTRC 85/15 ZrO_2/CoCrAlY
TMY-4	ZrO_2 +7% Y_2O_3	

TABLE 2

Sample Geometries, Masses and Bulk Density Values

Sample Designation	Thick (in.)	Width (in.)	Width (in.)	Mass (gms)	Density (gms cm^{-3})
JWC-1	0.1303	0.4825	0.4866	1.5479	3.088
JWC-2	0.1506	0.4951	0.5031	1.9231	3.128
JWC-3	0.1475	0.4885	0.4691	1.5881	2.867
JWC-4	0.1551	0.5010	0.4699	1.9018	3.178
JWC-5	0.1494	0.4868	0.5051	1.9114	3.157
JWC-6	0.1471	0.5005	0.5007	1.7399	2.880
JWC-7	0.1506	0.4778	0.4890	4.2667	7.400
JWC-8	0.1506	0.5003	0.4990	4.3853	7.118
TMY-1	0.0891	0.5062	0.5046	1.8031	4.835
TMY-2	0.1082	0.4850	0.4860	2.4822	5.939
TMY-3	0.0914	0.4777	0.4990	1.8609	5.212
TMY-4	0.0610	0.5042	0.4290	1.0619	4.911

TABLE 3

Specific Heat of Al_2TiO_5

TEMP. (C)	JWC-1 (Ws gm^{-1}K^{-1})	JWC-2 (Ws gm^{-1}K^{-1})	JWC-3 (Ws gm^{-1}K^{-1})	JWC-4 (Ws gm^{-1}K^{-1})	JWC-5 (Ws gm^{-1}K^{-1})	JWC-6 (Ws gm^{-1}K^{-1})
52.0	0.771	0.769	0.770	0.785	0.775	0.777
77.0	0.808	0.808	0.802	0.819	0.810	0.814
102.0	0.835	0.836	0.827	0.846	0.837	0.842
127.0	0.860	0.860	0.849	0.868	0.859	0.866
152.0	0.882	0.882	0.869	0.888	0.878	0.887
177.0	0.899	0.900	0.885	0.905	0.895	0.904
202.0	0.914	0.915	0.899	0.920	0.910	0.919
227.0	0.928	0.928	0.911	0.933	0.923	0.933
252.0	0.939	0.940	0.923	0.943	0.935	0.944
277.0	0.950	0.951	0.933	0.954	0.946	0.954
302.0	0.961	0.962	0.945	0.965	0.958	0.964
327.0	0.972	0.973	0.956	0.976	0.969	0.974
352.0	0.983	0.984	0.968	0.986	0.982	0.985
377.0	0.995	0.995	0.981	0.998	0.995	0.997
402.0	1.003	1.003	0.986	1.007	1.004	1.011
427.0	1.014	1.018	0.993	1.013	1.014	1.022
452.0	1.020	1.025	0.999	1.020	1.024	1.030
477.0	1.029	1.034	1.008	1.030	1.035	1.036
502.0	1.037	1.041	1.017	1.039	1.045	1.041
527.0	1.046	1.048	1.024	1.048	1.051	1.047
552.0	1.054	1.056	1.030	1.056	1.054	1.050
577.0	1.063	1.064	1.035	1.061	1.058	1.057

TABLE 4

Specific Heat of Iron and ZrO_2 Materials

TEMP. (C)	JWC-7 (Ws $gm^{-1}K^{-1}$)	JWC-8 (Ws $gm^{-1}K^{-1}$)	TMY-1 (Ws $gm^{-1}K^{-1}$)	TMY-2 (Ws $gm^{-1}K^{-1}$)	TMY-3 (Ws $gm^{-1}K^{-1}$)	TMY-4 (Ws $gm^{-1}K^{-1}$)
77.0	0.503	0.510	0.488	0.487	0.492	0.496
102.0	0.511	0.518	0.503	0.499	0.505	0.510
127.0	0.518	0.524	0.514	0.508	0.516	0.522
152 0	0.523	0.529	0.524	0.517	0.524	0.532
177.0	0.528	0.533	0.532	0.524	0.532	0.540
202 0	0.533	0.536	0.539	0.530	0.538	0.546
227.0	0.538	0.541	0.544	0.536	0.543	0.551
252 0	0.543	0.545	0.549	0.540	0.548	0.557
277.0	0.547	0.550	0.553	0.545	0.552	0.560
302 0	0.551	0.553	0.557	0.548	0.556	0.565
327.0	0.553	0.555	0.560	0.552	0.559	0.569
352.0	0.556	0.558	0.564	0.555	0.563	0.573
377.0	0.559	0.562	0.568	0.558	0.567	0.577
402.0	0.562	0.569	0.572	0.572	0.582	0.586
427.0	0.564	0.577	0.575	0.580	0.585	0.590
452 0	0.568	0.590	0.576	0.586	0.589	0.593
477.0	0.579	0.605	0.579	0.590	0.592	0.598
502 0	0.595	0.615	0.583	0.594	0.596	0.601
527.0	0.605	0.621	0.586	0.596	0.601	0.604
552.0	0.613	0.624	0.587	0.596	0.607	0.606
577.0	0.617	0.624	0.586	0.596	0.612	0.608

TABLE 5

Thermal Diffusivity Results

Temp. (°C)	JWC-1 (cm^2sec^{-1})	JWC-2 (cm^2sec^{-1})	JWC-3 (cm^2sec^{-1})	JWC-4 (cm^2sec^{-1})	JWC-5 (cm^2sec^{-1})	JWC-6 (cm^2sec^{-1})	JWC-7 (cm^2sec^{-1})	JWC-7 (cm^2sec^{-1})
300	0.00520	0.00572	0.00370	0.00527	0.00556	0.00378	0.0370	0.1060
600	0.00498	0.00536	0.00367	0.00491	0.00508	0.00384	0.0445	0.0703
700	0.00492	0.00530	0.00365	0.00480	0.00503	0.00382	0.0462	0.0556
800	0.00551	0.00517	0.00402	0.00488	0.00515	0.00429	0.0485	0.0580
900	0.00595	0.00611	0.00452	0.00535	0.00537	0.00470	0.0499	0.0708

Temp. (C)	TMY-1 (cm^2sec^{-1})	TMY-2 (cm^2sec^{-1})	TMY-3 (cm^2sec^{-1})	TMY-4 (cm^2sec^{-1})
315	0.00254	0.00563	0.00367	0.00417
400	0.00256	0.00571	0.00364	0.00393
500	0.00256	0.00568	0.00357	0.00375
600	0.00234	0.00565	0.00356	0.00375
700	0.00229	0.00555	0.00354	0.00361
800	0.00224	0.00565	0.00353	0.00359
870	0.00219	0.00565	0.00353	0.00352

TABLE 6

Thermal Conductivity Calculations

Sample (No.)	Temp. (C)	Density ($gm\ cm^{-3}$)	Specific Heat ($W\ s\ gm^{-1}\ K^{-1}$)	Diffusivity ($cm^2\ sec^{-1}$)	Conductivity ($W\ cm^{-1}\ K^{-1}$)	Conductivity (BTU units *)	Temp (F)
JWC-1	600.0	3.088	1.0710	0.00496	0.01640	11.37	1112.0
JWC-1	700.0	3.088	1.1050	0.00500	0.01706	11.83	1292.0
JWC-1	800.0	3.088	1.1370	0.00537	0.01885	13.07	1472.0
JWC-1	900.0	3.088	1.1680	0.00545	0.01966	13.63	1652.0
JWC-2	600.0	3.128	1.0710	0.00540	0.01809	12.54	1112.0
JWC-2	700.0	3.128	1.1050	0.00530	0.01832	12.70	1292.0
JWC-2	800.0	3.128	1.1370	0.00516	0.01835	12.72	1472.0
JWC-2	900.0	3.128	1.1680	0.00605	0.02210	15.33	1652.0
JWC-3	600.0	2.867	1.0460	0.00367	0.01101	7.63	1112.0
JWC-3	700.0	2.867	1.0770	0.00364	0.01124	7.79	1292.0
JWC-3	800.0	2.867	1.1060	0.00402	0.01275	8.84	1472.0
JWC-3	900.0	2.867	1.1270	0.00452	0.01460	10.13	1652.0
JWC-4	600.0	3.178	1.0710	0.00491	0.01671	11.59	1112.0
JWC-4	700.0	3.178	1.1050	0.00480	0.01686	11.69	1292.0
JWC-4	800.0	3.178	1.1370	0.00488	0.01763	12.23	1472.0
JWC-4	900.0	3.178	1.1680	0.00535	0.01986	13.77	1652.0
JWC-5	600.0	3.157	1.0710	0.00508	0.01718	11.91	1112.0
JWC-5	700.0	3.157	1.1050	0.00503	0.01755	12.17	1292.0
JWC-5	800.0	3.157	1.1370	0.00513	0.01841	12.77	1472.0
JWC-5	900.0	3.157	1.1680	0.00538	0.01984	13.75	1652.0
JWC-6	600.0	2.880	1.0710	0.00378	0.01166	8.08	1112.0
JWC-6	700.0	2.880	1.1050	0.00384	0.01222	8.47	1292.0
JWC-6	800.0	2.880	1.1370	0.00427	0.01398	9.69	1472.0
JWC-6	900.0	2.880	1.1680	0.00465	0.01564	10.85	1652.0

* (BTU in hr^{-1} ft^{-2} F^{-1})

TABLE 6 (Cont.)

Thermal Conductivity Calculations

Sample (No.)	Temp. (C)	Density ($gm\ cm^{-3}$)	Specific Heat ($W\ s\ gm^{-1}\ K^{-1}$)	Diffusivity ($cm^2\ sec^{-1}$)	Conductivity ($W\ cm^{-1}\ K^{-1}$)	Conductivity (BTU units *)	Temp (F)
JWC-7	600.0	7.400	0.6270	0.04450	0.20647	143.16	1112.0
JWC-7	700.0	7.400	0.6400	0.04620	0.21880	151.71	1292.0
JWC-7	800.0	7.400	0.6580	0.04850	0.23616	163.74	1472.0
JWC-7	900.0	7.400	0.6810	0.04990	0.25147	174.35	1652.0
JWC-8	600.0	7.118	0.6270	0.07030	0.31375	217.54	1112.0
JWC-8	700.0	7.118	0.6670	0.05560	0.26397	183.02	1292.0
JWC-8	800.0	7.118	0.6800	0.05800	0.28073	194.65	1472.0
JWC-8	900.0	7.118	0.6560	0.07060	0.33059	229.22	1652.0
TMY-1	315.0	4.835	0.5580	0.00254	0.00685	4.75	599.0
TMY-1	400.0	4.835	0.5720	0.00256	0.00708	4.91	752.0
TMY-1	500.0	4.835	0.5830	0.00256	0.00722	5.00	932.0
TMY-1	600.0	4.835	0.5880	0.00234	0.00665	4.61	1112.0
TMY-1	700.0	4.835	0.5930	0.00229	0.00657	4.55	1292.0
TMY-1	800.0	4.835	0.5950	0.00224	0.00644	4.47	1472.0
TMY-1	870.0	4.835	0.5970	0.00219	0.00632	4.38	1598.0
TMY-2	315.0	5.939	0.5500	0.00563	0.01839	12.75	599.0
TMY-2	400.0	5.939	0.5720	0.00571	0.01940	13.45	752.0
TMY-2	500.0	5.939	0.5940	0.00568	0.02004	13.89	932.0
TMY-2	600.0	5.939	0.6010	0.00565	0.02017	13.98	1112.0
TMY-2	700.0	5.939	0.6070	0.00555	0.02001	13.87	1292.0
TMY-2	800.0	5.939	0.6100	0.00565	0.02047	14.19	1472.0
TMY-2	870.0	5.939	0.6150	0.00565	0.02064	14.31	1598.0
TMY-3	315.0	5.212	0.5570	0.00367	0.01065	7.39	599.0
TMY-3	400.0	5.212	0.5820	0.00364	0.01104	7.66	752.0
TMY-3	500.0	5.212	0.5960	0.00357	0.01109	7.69	932.0
TMY-3	600.0	5.212	0.6070	0.00356	0.01126	7.81	1112.0
TMY-3	700.0	5.212	0.6120	0.00354	0.01129	7.83	1292.0
TMY-3	800.0	5.212	0.6170	0.00353	0.01135	7.87	1472.0
TMY-3	870.0	5.212	0.6220	0.00353	0.01144	7.93	1598.0
TMY-4	315.0	4.911	0.5660	0.00417	0.01159	8.04	599.0
TMY-4	400.0	4.911	0.5860	0.00393	0.01131	7.84	752.0
TMY-4	500.0	4.911	0.6010	0.00375	0.01107	7.67	932.0
TMY-4	600.0	4.911	0.6070	0.00375	0.01118	7.75	1112.0
TMY-4	700.0	4.911	0.6120	0.00361	0.01085	7.52	1292.0
TMY-4	800.0	4.911	0.6170	0.00359	0.01088	7.54	1472.0
TMY-4	870.0	4.911	0.6220	0.00352	0.01075	7.46	1598.0

* (BTU $in\ hr^{-1}\ ft^{-2}\ F^{-1}$)

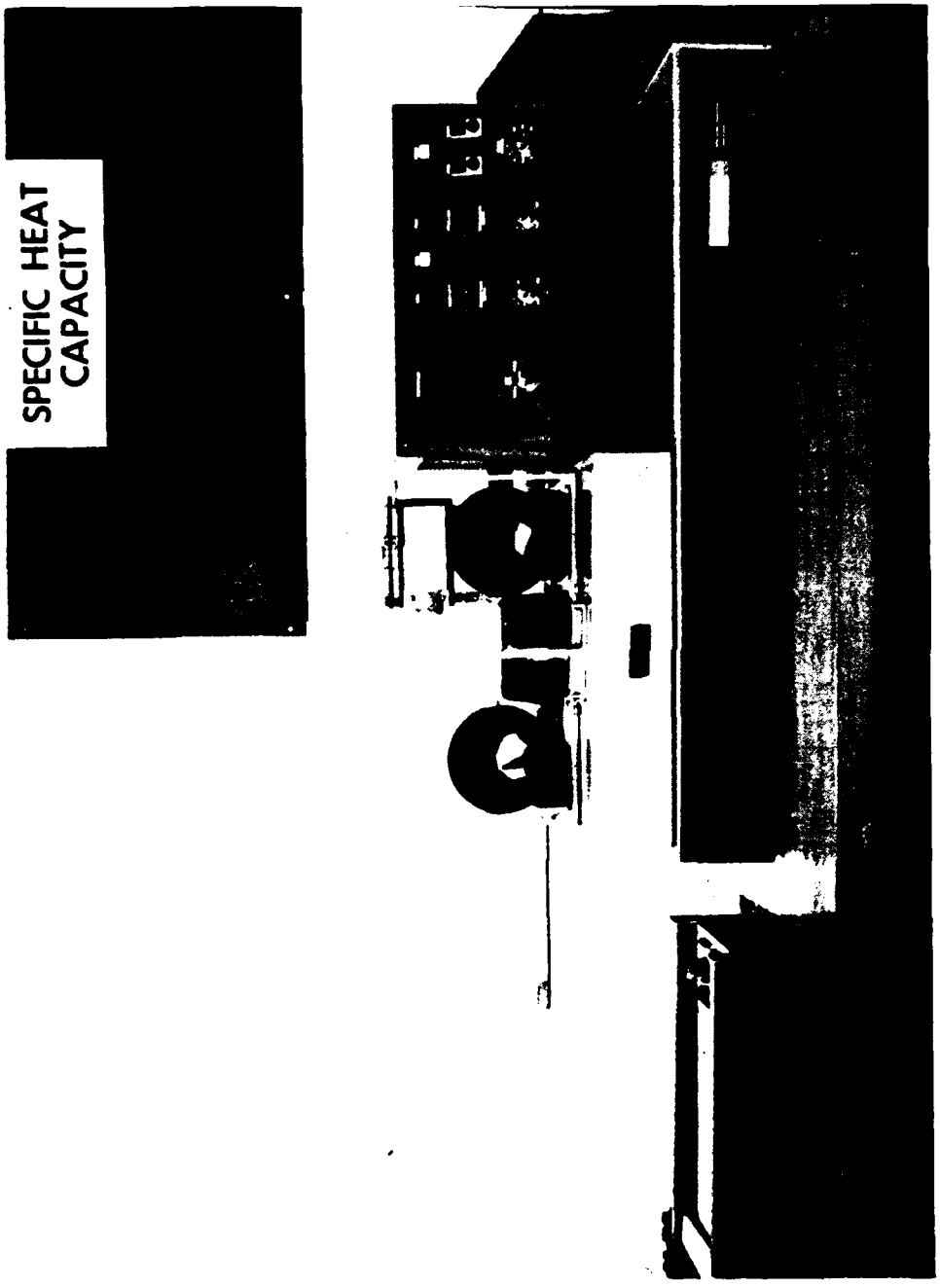

Figure 1. Differential Scanning Calorimeter

Figure 2. Digital Data Acquisition System

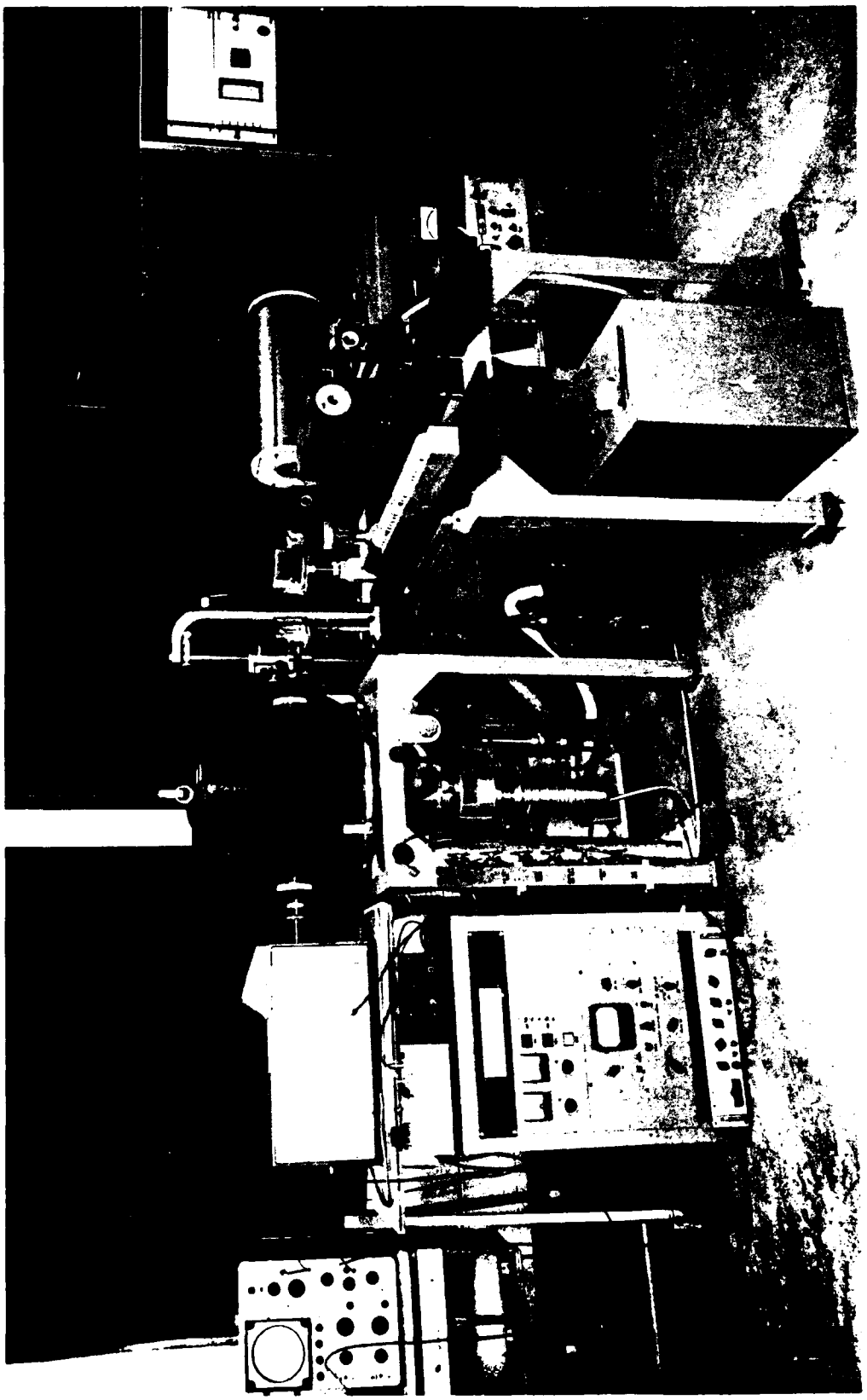

Figure 3. Flash Diffusivity Apparatus

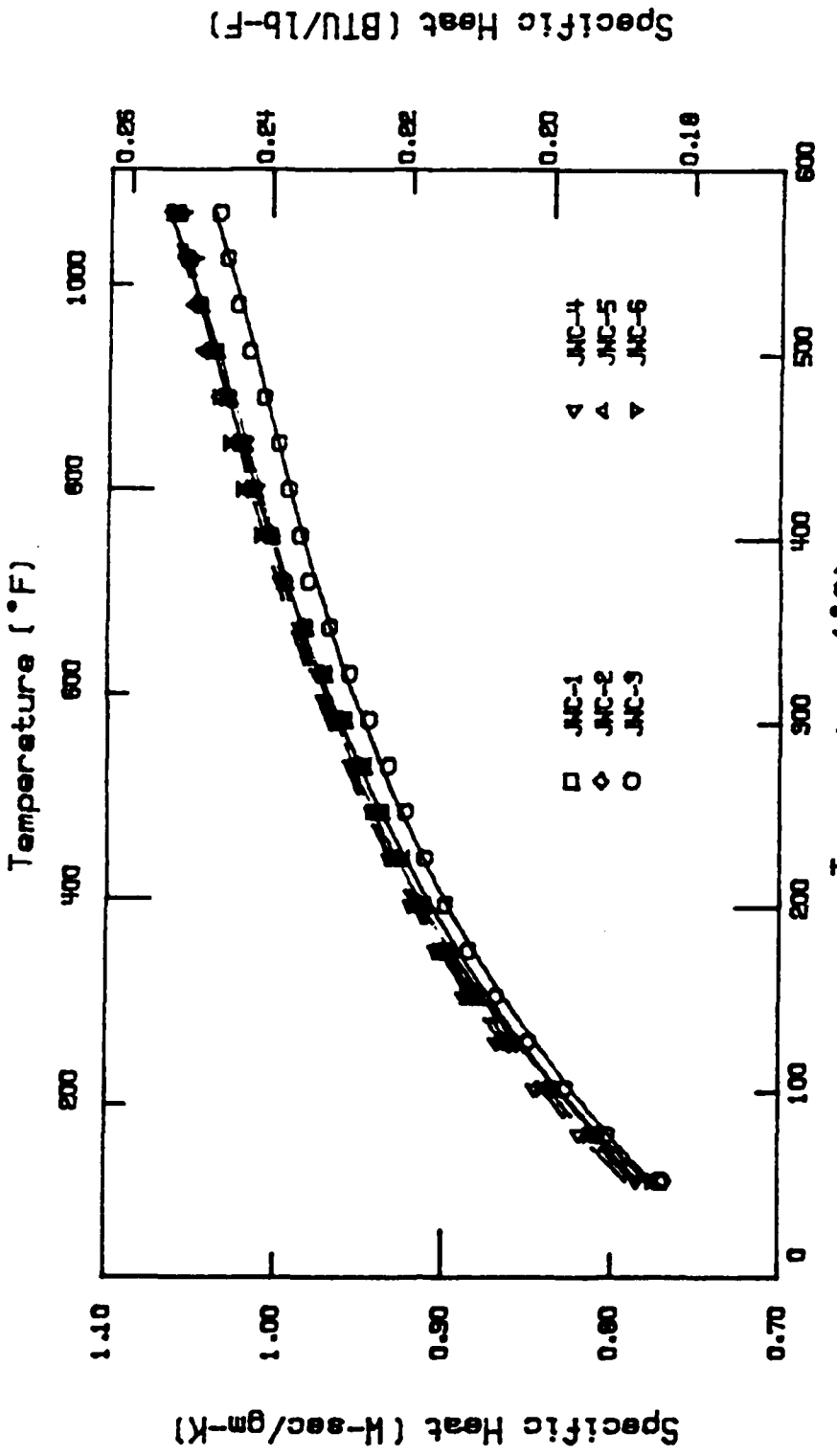

Figure 4. Specific Heat (Samples JWC 1 - 6)

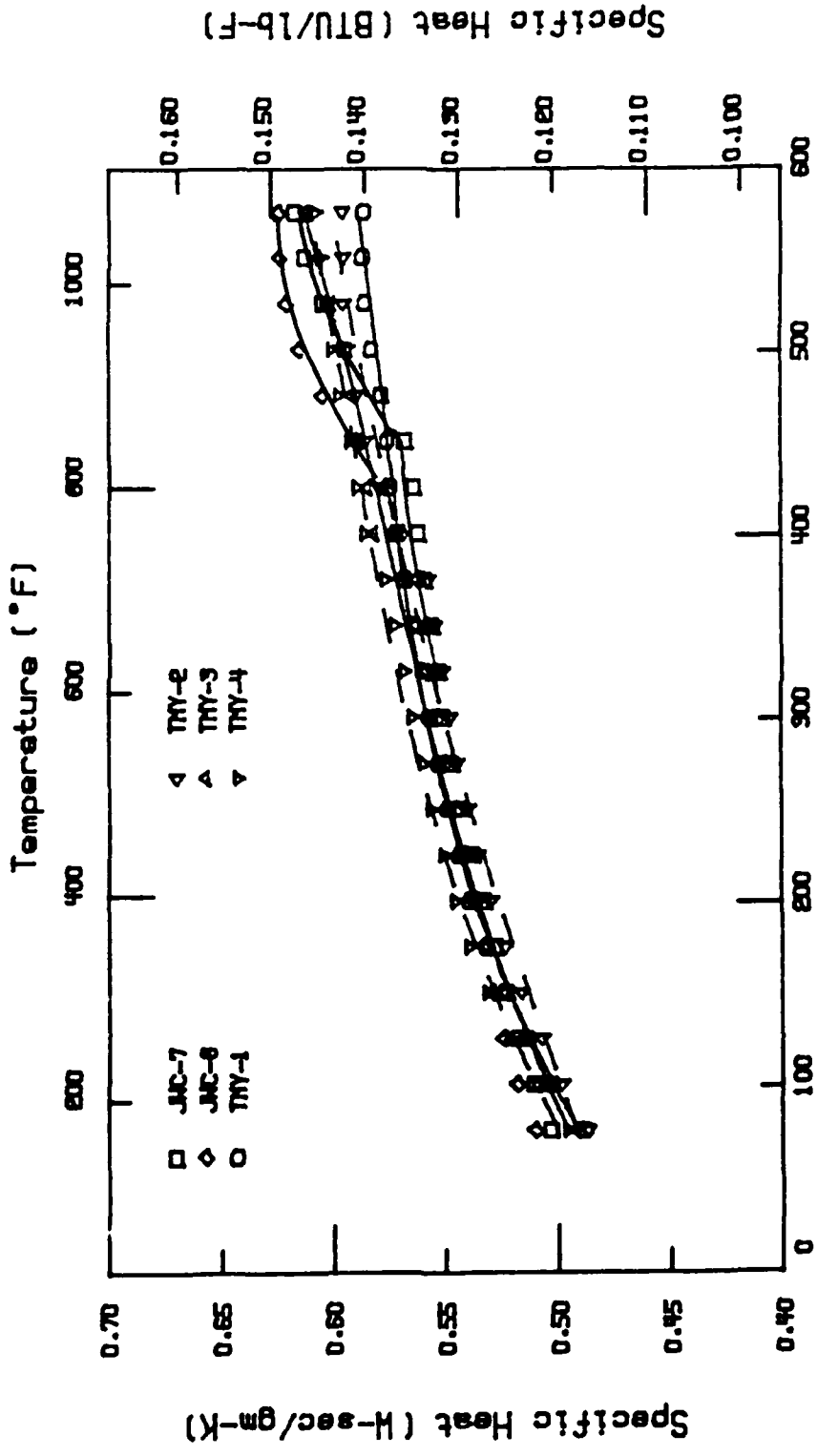

Figure 5. Specific Heat (Samples JWC 7, 8 and TMY 1 - 4)

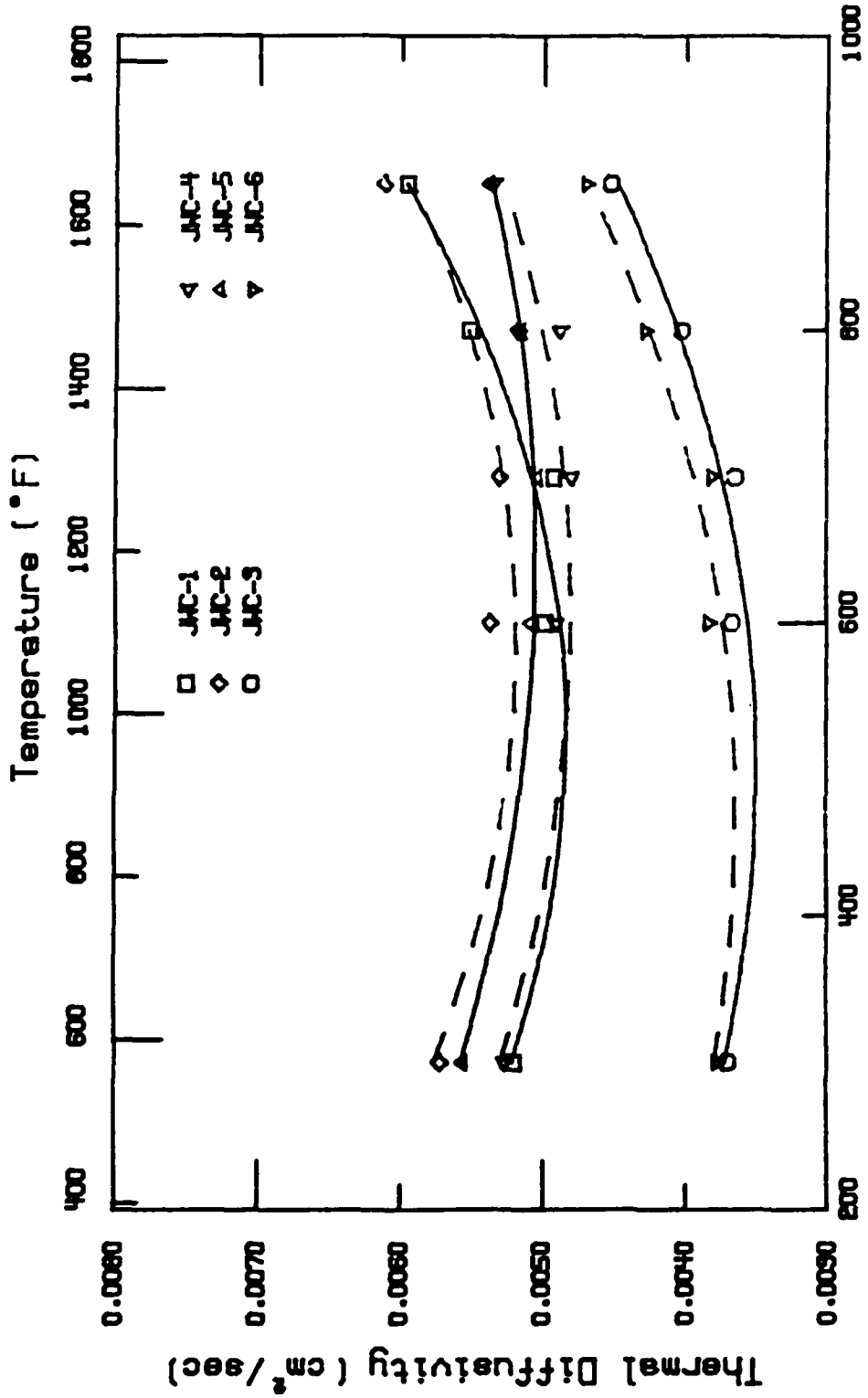

Figure 6. Thermal Diffusivity (Samples JWC 1 - 6)

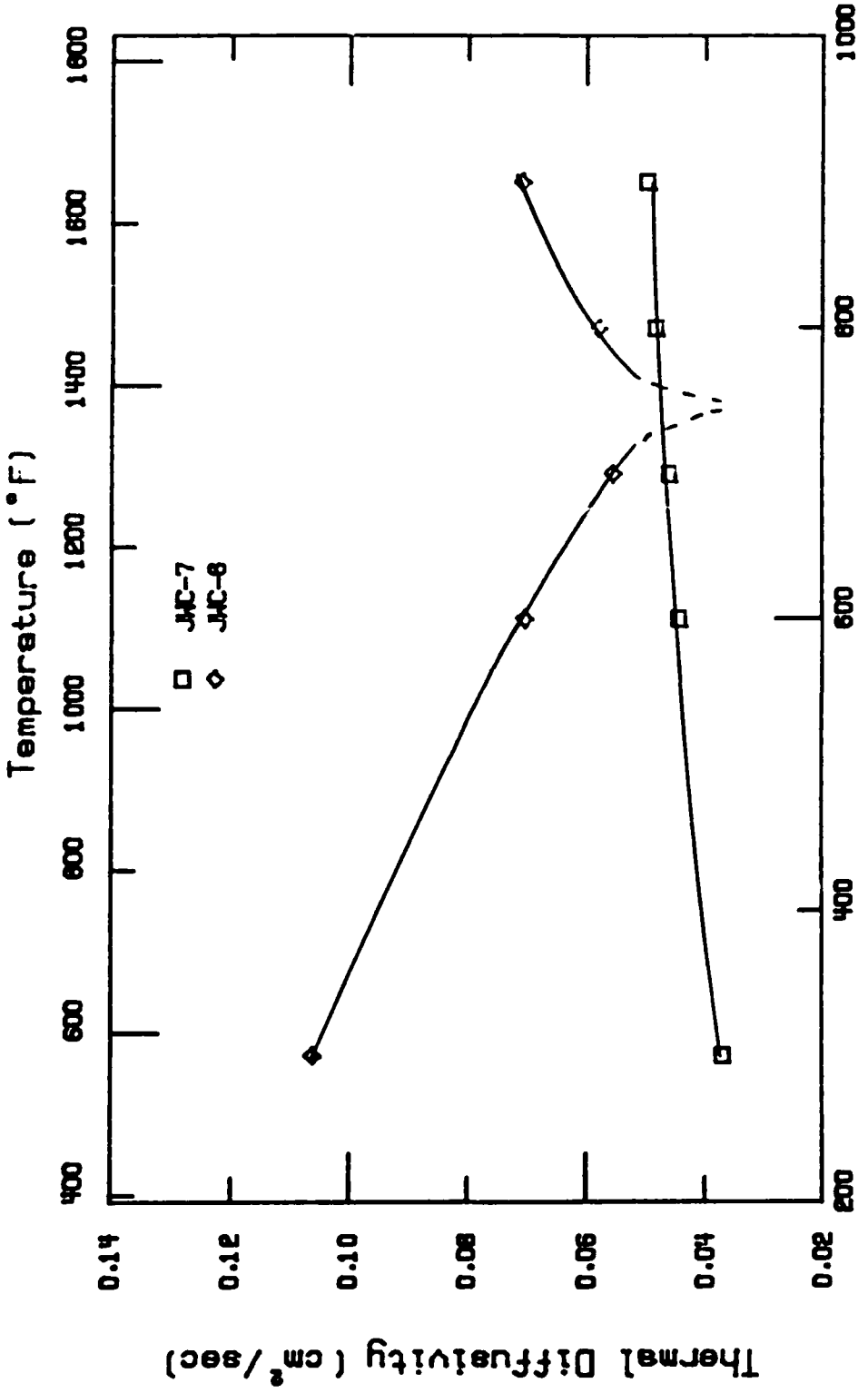

Figure 7. Thermal Diffusivity (Samples JWC 7 and 8)

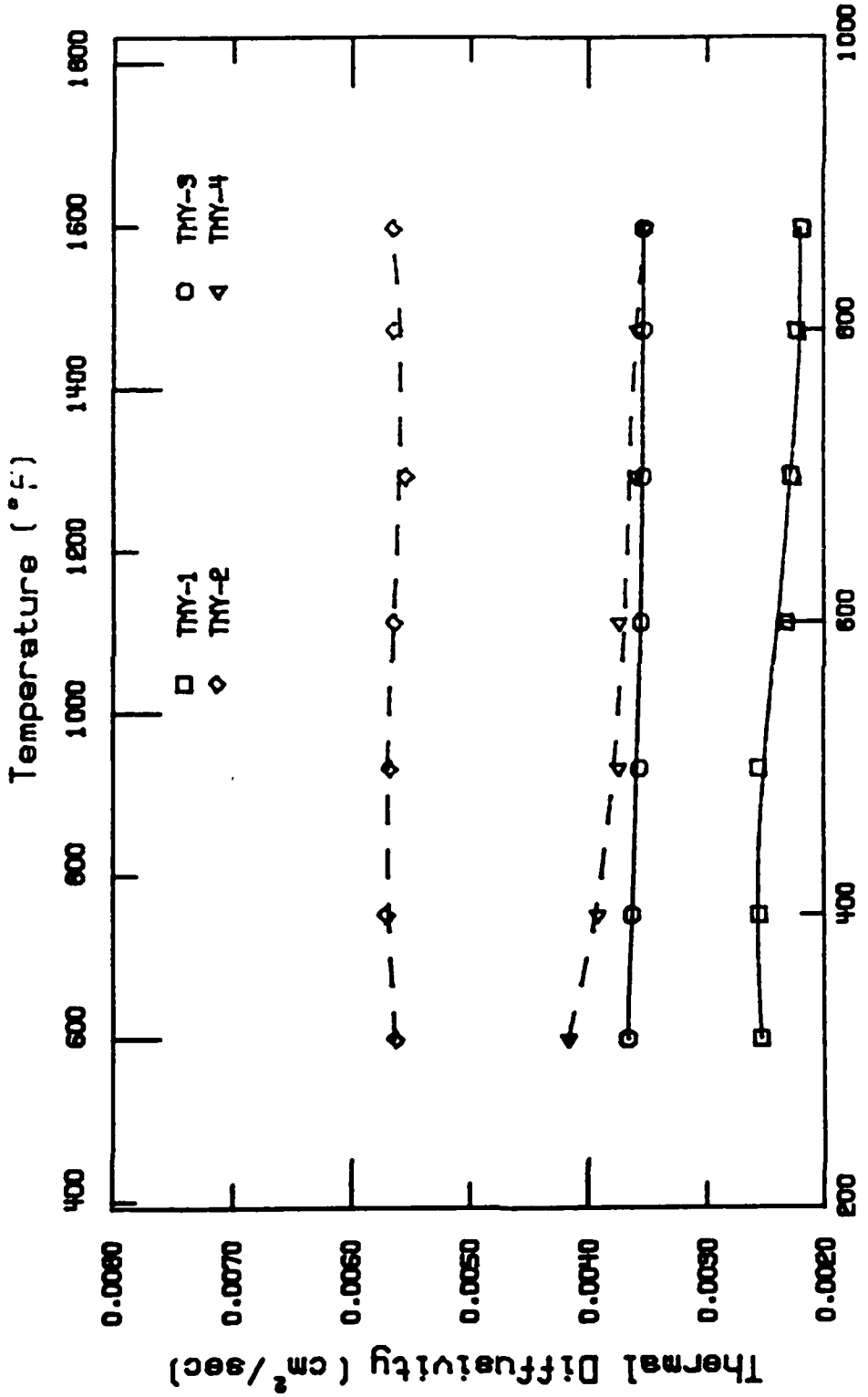

Figure 8. Thermal Diffusivity (Samples TMY 1 - 4)

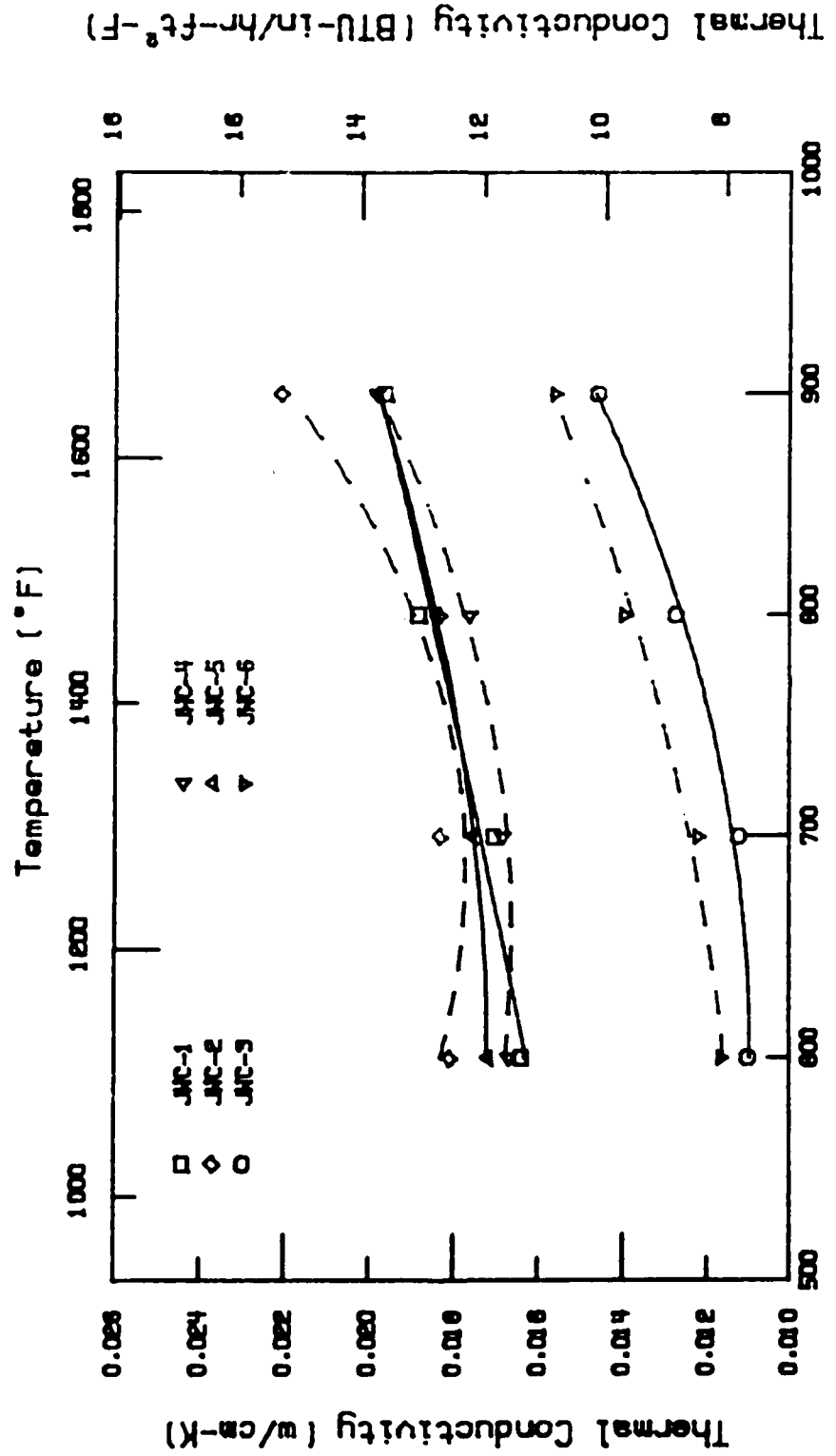

Figure 9. Thermal Conductivity (Samples JWC 1 - 6)

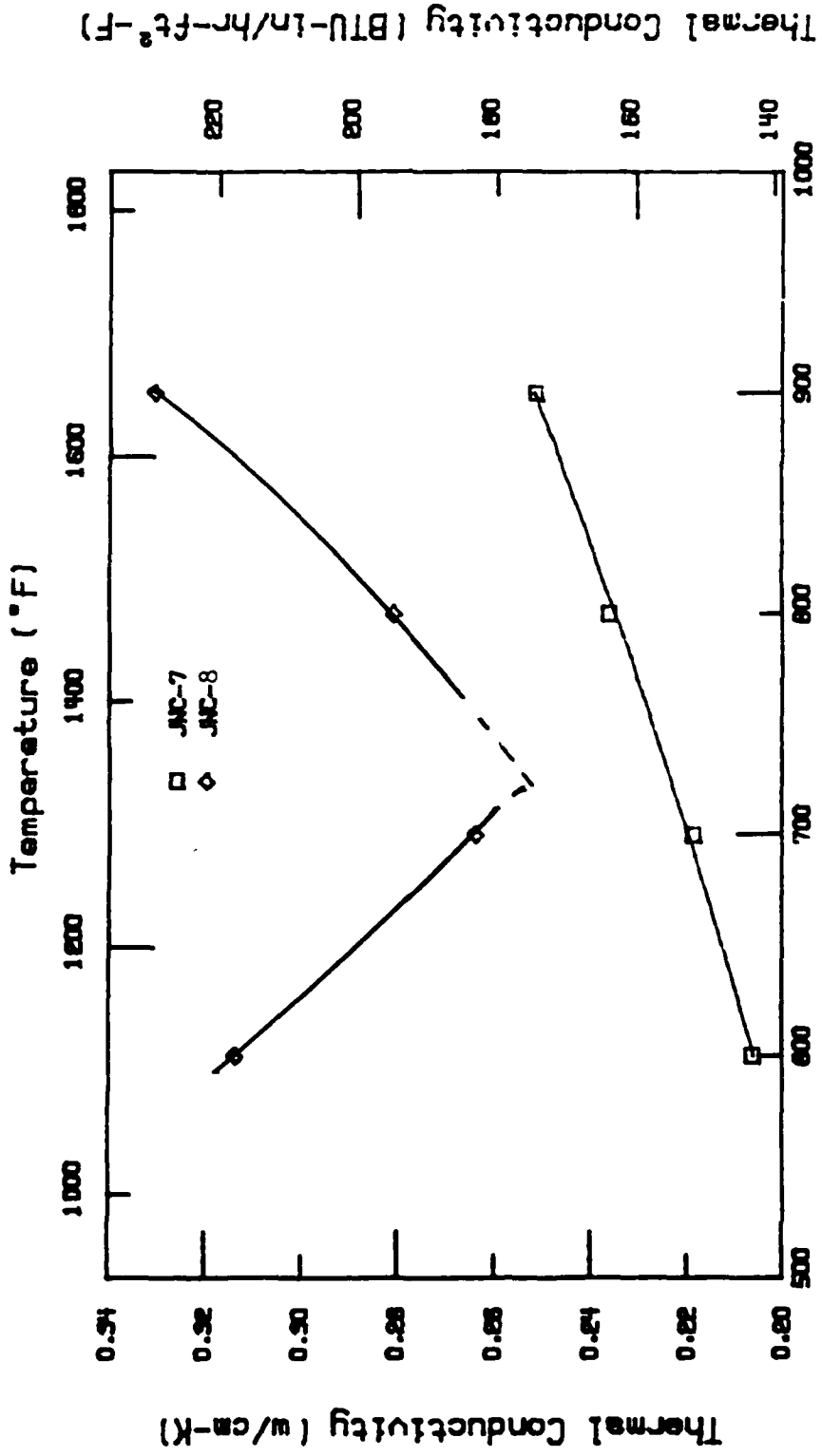

Figure 10. Thermal Conductivity (Samples JWC 7 and 8)

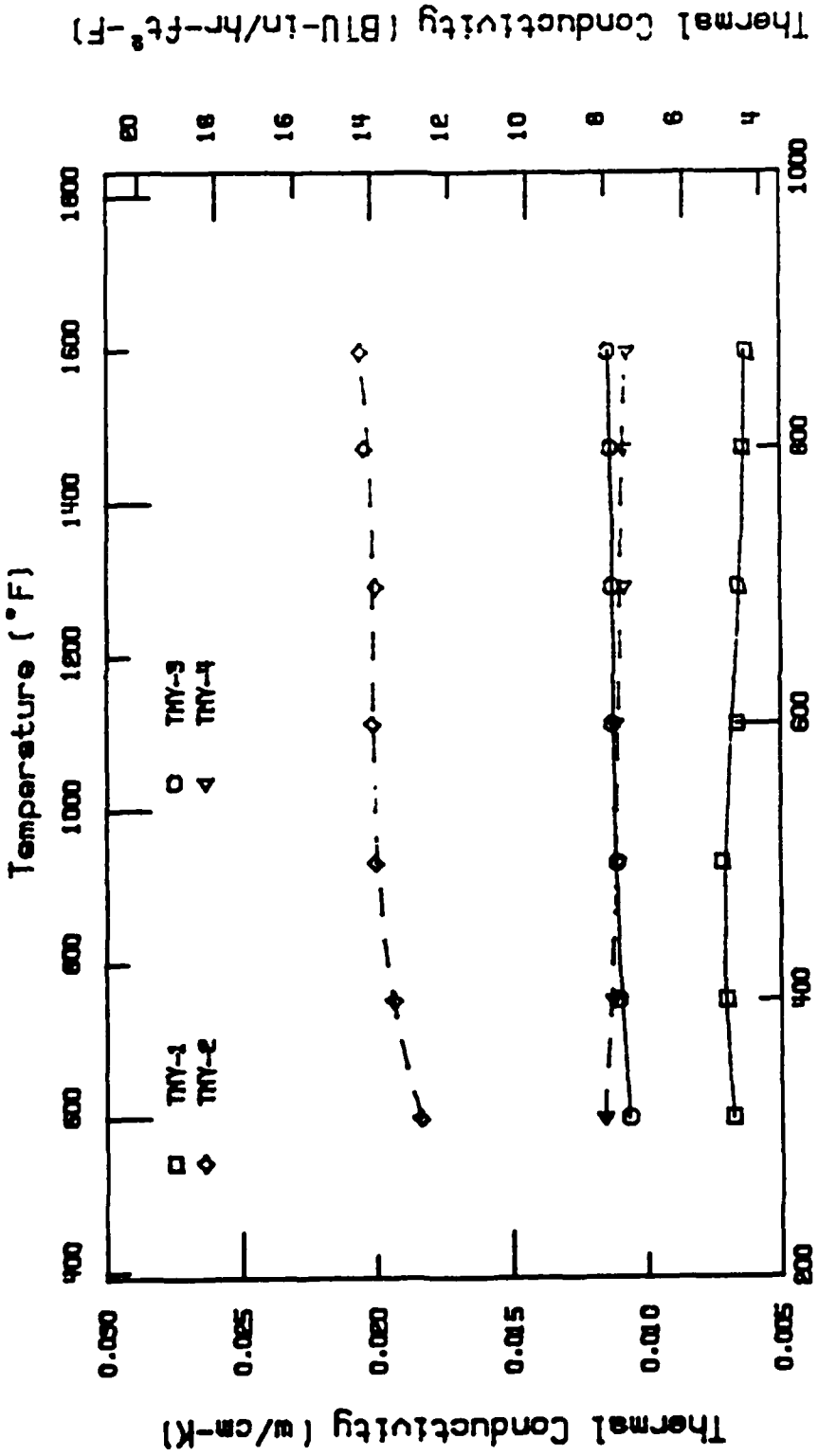

Figure 11. Thermal Conductivity (Samples TMY 1 - 4)

DISTRIBUTION LIST

No. of Copies	To
1	Office of the Under Secretary of Defense for Research and Engineering, The Pentagon, Washington, DC 20301
	Commander, U.S. Army Laboratory Command, 2800 Powder Mill Road, Adelphi, MD 20783-1145
1	ATTN: AMSLC-IM-TL
1	AMSLC-CT
	Commander, Defense Technical Information Center, Cameron Station, Building 5, 5010 Duke Street, Alexandria, VA 22304-6145
2	ATTN: DTIC-FDAC
1	Metals and Ceramics Information Center, Battelle Columbus Laboratories, 505 King Avenue, Columbus, OH 43201
	Commander, Army Research Office, P.O. Box 12211, Research Triangle Park, NC 27709-2211
1	ATTN: Information Processing Office
	Commander, U.S. Army Materiel Command, 5001 Eisenhower Avenue, Alexandria, VA 22333
1	ATTN: AMCLD
	Commander, U.S. Army Materiel Systems Analysis Activity, Aberdeen Proving Ground, MD 21005
1	ATTN: AMXSY-MP, H. Cohen
	Commander, U.S. Army Missile Command, Redstone Scientific Information Center, Redstone Arsenal, AL 35898-5241
1	ATTN: AMSMI-RD-CS-R/Doc
1	AMSMI-RLM
	Commander, U.S. Army Armament, Munitions and Chemical Command, Dover, NJ 07801
2	ATTN: Technical Library
1	AMDAR-LCA, Mr. Harry E. Pebly, Jr., PLASTEC, Director
	Commander, U.S. Army Natick Research, Development and Engineering Center, Natick, MA 01760
1	ATTN: Technical Library
	Commander, U.S. Army Satellite Communications Agency, Fort Monmouth, NJ 07703
1	ATTN: Technical Document Center
	Commander, U.S. Army Tank-Automotive Command, Warren, MI 48397-5000
1	ATTN: AMSTA-ZSK
2	AMSTA-TSL, Technical Library
	Commander, White Sands Missile Range, NM 88002
1	ATTN: STEWS-WS-VT
	President, Airborne, Electronics and Special Warfare Board, Fort Bragg, NC 28307
1	ATTN: Library
	Director, U.S. Army Ballistic Research Laboratory, Aberdeen Proving Ground, MD 21005
1	ATTN: SLCBR-TSB-S (STINFO)
	Commander, Dugway Proving Ground, Dugway, UT 84022
1	ATTN: Technical Library, Technical Information Division
	Commander, Harry Diamond Laboratories, 2800 Powder Mill Road, Adelphi, MD 20783
1	ATTN: Technical Information Office
	Director, Benet Weapons Laboratory, LCWSL, USA AMCCOM, Watervliet, NY 12189
1	ATTN: AMSMC-LCB-TL
1	AMSMC-LCB-R
1	AMSMC-LCB-RM
1	AMSMC-LCB-RP
	Commander, U.S. Army Foreign Science and Technology Center, 220 7th Street, N.E., Charlottesville, VA 22901-5396
3	ATTN: AIFRTC, Applied Technologies Branch, Gerald Schlesinger

No. of Copies	To
	Commander, U.S. Army Aeromedical Research Unit, P.O. Box 577, Fort Rucker, AL 36360
1	ATTN: Technical Library
	Commander, U.S. Army Aviation Systems Command, Aviation Research and Technology Activity, Aviation Applied Technology Directorate, Fort Eustis, VA 23604-5577
1	ATTN: SAVDL-E-MOS
	U.S. Army Aviation Training Library, Fort Rucker, AL 36360
1	ATTN: Building 5906-5907
	Commander, U.S. Army Agency for Aviation Safety, Fort Rucker, AL 36362
1	ATTN: Technical Library
	Commander, USACDC Air Defense Agency, Fort Bliss, TX 79916
1	ATTN: Technical Library
	Commander, U.S. Army Engineer School, Fort Belvoir, VA 22060
1	ATTN: Library
	Commander, U.S. Army Engineer Waterways Experiment Station, P. O. Box 631, Vicksburg, MS 39180
1	ATTN: Research Center Library
	Commandant, U.S. Army Quartermaster School, Fort Lee, VA 23801
1	ATTN: Quartermaster School Library
	Naval Research Laboratory, Washington, DC 20375
1	ATTN: Code 5830
2	Dr. G. R. Yoder - Code 6384
	Chief of Naval Research, Arlington, VA 22217
1	ATTN: Code 471
1	Edward J. Morrissey, WRDC/MLTE, Wright-Patterson Air Force, Base, OH 45433-6523
	Commander, U.S. Air Force Wright Research & Development Center, Wright-Patterson Air Force Base, OH 45433-6523
1	ATTN: WRDC/MLC
1	*WRDC/MLLP, M. Forney, Jr.*
1	WRDC/MLBC, Mr. Stanley Schulman
	National Aeronautics and Space Administration, Marshall Space Flight Center, Huntsville, AL 35812
1	ATTN: R. J. Schwinghammer, EH01, Dir, M&P Lab
1	Mr. W. A. Wilson, EH41, Bldg. 4612
	U.S. Department of Commerce, National Institute of Standards and Technology, Gaithersburg, MD 20899
1	ATTN: Stephen M. Hsu, Chief, Ceramics Division, Institute for Materials Science and Engineering
1	Committee on Marine Structures, Marine Board, National Research Council, 2101 Constitution Ave., N.W., Washington, DC 20418
1	Librarian, Materials Sciences Corporation, Guynedd Plaza II, Bethlehem Pike, Spring House, PA 19477
1	The Charles Stark Draper Laboratory, 68 Albany Street, Cambridge, MA 02139
	Wyman-Gordon Company, Worcester, MA 01601
1	ATTN: Technical Library
	Lockheed-Georgia Company, 86 South Cobb Drive, Marietta, GA 30063
1	ATTN: Materials and Processes Engineering Dept. 71-11, Zone 54
	General Dynamics, Convair Aerospace Division, P.O. Box 748, Fort Worth, TX 76101
1	ATTN: Mfg. Engineering Technical Library
1	Mechanical Properties Data Center, Belfour Stulen Inc., 13917 W. Bay Shore Drive, Traverse City, MI 49684
	Director, U.S. Army Materials Technology Laboratory, Watertown, MA 02172-0001
2	ATTN: SLCMT-TML
1	SLCMT-IMA-V
1	SLCMT-PR
10	SLCMT-EMC, J. Swab, COR

SUPPLEMENTAL DISTRIBUTION LIST

Jerome L. Ackerman, PhD
Director, NMR Spectroscopy
Massachusetts General Hospital
NMR Center
149 13th Street
Charlestown, MA 02129

Dr. Maurice F. Amateau
Applied Research Laboratory
P.O. Box 30
State College, PA 16804

Dr. Clifford Ballard
Manager - Ceramic Program
Allied-Signal Inc.
P.O. Box 1021R
Morristown, NJ 07960

Dr. Ron Bhatt
US Army Aviation Systems Command
Propulsion Division
NASA Lewis Research Center
21000 Brookpark Road (MS 77-12)
Cleveland, Ohio 44135-3191

SACO Defense, Inc.
291 North Street
Saco, ME 04072
ATTN: Seth Bredbury

Prof. Paul Calvert
University of Arizona
Dept. of Materials Science & Engineering
Tucson, AZ 85721

Dr. Gary Crosbie
1430 Culver
Dearborn, MI 48124-4036

Dr. Matt Ferber
ORNL
P.O. Box 2008
Oak Ridge, Tenn 37830

Prof. John Haggerty
Mass. Institute of Technology
Industrial Liaison Program
RM E38-400
292 Main Street
Cambridge, MA 02139

Dr. James Hannoosh
CERBEC Ceramic Bearing Co.
10 Airport Park Rd.
East Granby, CT 06026

Mr. Dewey Heichel
Six W. Hollow Ln.
Webster, MA 01570

Mr. Roy Kamo
Adiabatics Inc.
630 South Mapleton
Columbus, Indiana 47201

Dr. Keith Karasek
Ceramics Group
Allied-Signal Research & Technology
50 East Algonquin Road
Des Plaines, IL 60016

Dr. Lisa Klein
Rutgers University
Dept. of Ceramics
Box 909
Piscataway, NJ 08855-0909

William Koenigsburg
GTE Laboratories
40 Sylvan Road
Waltham, MA 02254

Dr. Richard Laine
University of Washington
255 Wilcox Hall FB-10
Seattle, WA 98195

Dr. David Larson
Materials Research Department
Corning Glass Works
Sullivan Park
Corning, NY 14831

Dr. Jean-Francois LeCostaouec
Textron Specialty Materials
2 Industrial Ave.
Lowell, MA 01851

Dr. David Lewis
Code 6360
Naval Research Lab
Washington, DC 20375

Dr. William Long
ESK Engineered Ceramics
Ten Tunxis Trail, N
West Redding, CT 06896

Dr. Nguien Minh
AiResearch Los Angeles Division
2525 W. 190th Street
P.O. Box 2960
Torrance, CA 90509

Dr. Peter E.D. Morgan
Rockwell International Science Ctr.
1049 Camino dos Rios
Box 1085
Thousand Oaks, CA 91360

Mr. Richard Palicka
CERCOM, Inc.
1960 Watson Way
Vista, CA 92083

Mr. Donald Paterson
Engineering Analysis & Test Dept.
Raytheon Missile Systems
50 Apple Hill Drive
Tewksbury, MA 01876-0901

Dr. Harry I. Ringermacher
United Technology Research Center
Mail Stop 86
Silver Lane
E. Hartford, CT 06108

Dr. Doug Rose
Tank Automotive Command
ATTN: AMSTA-RG
Warren, MI 48397-5000

Dr. William Sanders
NASA Lewis Research Center
M.S. 49-3
21000 Brookpark Road
Cleveland, Ohio 44135

Mr. Brian Seegmiller
Coors Ceramics
17750 West 32nd Ave.
Golden, CO 80401

Dr. Raj Singh
General Electric Co.
R&D Center
BLDG. K1-Room 4A32
P.O. Box 8
Schenectady, NY 12301

Mr. Frank Skeele
Dow Chemical Co.
Central Research
Advanced Ceramics Laboratory
1776 Building
Midland, NI 48674

Dr. Roger Storm
Carborundum Company
Box 832
Niagara Falls, NY 14302

Dr. Richard Strehlow
Oak Ridge National Laboratory
Box 2008
Bldg. 4508
Oak Ridge, TN 37831-6088

Prof. Robert L. Thomas
Director, Manufacturing Research Inst.
Dept. of Physics and Astronomy
Wayne State University
Detroit, MI 48202

Prof. Thomas Vasilos
University of Lowell
Dept. of Chemical Engineering
Lowell, MA 01854

Dr. Larry Zawada
US Air Force Materials Lab
WRDC/MLLN
Wright Patterson AFB, 45433-6533

Dr. R.N. Katz
Mechanical Engineering Dept.
Worcester Polytechnic Institute
Worcester, MA 01760

Dr. Alex Vary
NASA Lewis Research Center
MS 6-1
21000 Brookpark Road
Cleveland, OH 44135

Dr. Russell Yeckley
Norton/TRW Ceramics
Goddard Road
Northboro, MA 01532

D. Ray Johnson
ORNL
P.O. Box 2008
Oak Ridge, TN 37830

R.B. Schulz
Advanced Materials Development
Department of Energy
1000 Independence Ave SW
Washington, DC 20585

U. S. Army Materials Technology Laboratory
Watertown, Massachusetts 02172-0001
Effect of Casting Procedures and
Diesel Engine Environment On the Behavior of
Aluminum Titanate
R. J. Stafford, J. W. Cogburn, and T. M. Yonushonis
Cummins Engine Company, Inc.
Columbus, IN 47202-3005
Technical Report MTL TR 90-20, April 1990
Contract DAAL04-87-C-0085
D/A Project: 1L162105.AH84

AD_____
Unclassified
Limited Distribution

KEY WORDS
Aluminum Titanate
Casting Procedures
Diesel Engines
Mechanical Properties
Thermophysical Properties
Exhaust Ports

The purpose of this report is to document the final results and conclusions of work on the behavior of aluminum titanate materials in a diesel engine environment.

Aluminum titanate materials from three different manufacturers showed significant differences in strength, stability and thermophysical properties. One material was low density with low strength, modulus and conductivity. The second material exhibited degradation to a -Al_2O_3 after aging at temperatures greater than 1000°C. The third material had very high strength as received but showed a strength loss of up to 40% after aging. However, the strength for this material after aging remained greater than the as-received strength of the other two materials.

Casting studies showed that cast-in-place ports can be produced. The most promising results were seen when the core sand composition was 50% SiC/50% Fe. The composition had thermal expansion characteristics which kept the core sand in contact with the aluminum titanate port during solidification and cooling of the cast iron.

U. S. Army Materials Technology Laboratory
Watertown, Massachusetts 02172-0001
Effect of Casting Procedures and
Diesel Engine Environment On the Behavior of
Aluminum Titanate
R. J. Stafford, J. W. Cogburn, and T. M. Yonushonis
Cummins Engine Company, Inc.
Columbus, IN 47202-3005
Technical Report MTL TR 90-20, April 1990
Contract DAAL04-87-C-0085
D/A Project: 1L162105.AH84

AD_____
Unclassified
Limited Distribution

KEY WORDS
Aluminum Titanate
Casting Procedures
Diesel Engines
Mechanical Properties
Thermophysical Properties
Exhaust Ports

The purpose of this report is to document the final results and conclusions of work on the behavior of aluminum titanate materials in a diesel engine environment.

Aluminum titanate materials from three different manufacturers showed significant differences in strength, stability and thermophysical properties. One material was low density with low strength, modulus and conductivity. The second material exhibited degradation to a -Al_2O_3 after aging at temperatures greater than 1000°C. The third material had very high strength as received but showed a strength loss of up to 40% after aging. However, the strength for this material after aging remained greater than the as-received strength of the other two materials.

Casting studies showed that cast-in-place ports can be produced. The most promising results were seen when the core sand composition was 50% SiC/50% Fe. The composition had thermal expansion characteristics which kept the core sand in contact with the aluminum titanate port during solidification and cooling of the cast iron.

U. S. Army Materials Technology Laboratory
Watertown, Massachusetts 02172-0001
Effect of Casting Procedures and
Diesel Engine Environment On the Behavior of
Aluminum Titanate
R. J. Stafford, J. W. Cogburn, and T. M. Yonushonis
Cummins Engine Company, Inc.
Columbus, IN 47202-3005
Technical Report MTL TR 90-20, April 1990
Contract DAAL04-87-C-0085
D/A Project: 1L162105.AH84

AD_____
Unclassified
Limited Distribution

KEY WORDS
Aluminum Titanate
Casting Procedures
Diesel Engines
Mechanical Properties
Thermophysical Properties
Exhaust Ports

The purpose of this report is to document the final results and conclusions of work on the behavior of aluminum titanate materials in a diesel engine environment.

Aluminum titanate materials from three different manufacturers showed significant differences in strength, stability and thermophysical properties. One material was low density with low strength, modulus and conductivity. The second material exhibited degradation to a -Al_2O_3 after aging at temperatures greater than 1000°C. The third material had very high strength as received but showed a strength loss of up to 40% after aging. However, the strength for this material after aging remained greater than the as-received strength of the other two materials.

Casting studies showed that cast-in-place ports can be produced. The most promising results were seen when the core sand composition was 50% SiC/50% Fe. The composition had thermal expansion characteristics which kept the core sand in contact with the aluminum titanate port during solidification and cooling of the cast iron.

U. S. Army Materials Technology Laboratory
Watertown, Massachusetts 02172-0001
Effect of Casting Procedures and
Diesel Engine Environment On the Behavior of
Aluminum Titanate
R. J. Stafford, J. W. Cogburn, and T. M. Yonushonis
Cummins Engine Company, Inc.
Columbus, IN 47202-3005
Technical Report MTL TR 90-20, April 1990
Contract DAAL04-87-C-0085
D/A Project: 1L162105.AH84

AD_____
Unclassified
Limited Distribution

KEY WORDS
Aluminum Titanate
Casting Procedures
Diesel Engines
Mechanical Properties
Thermophysical Properties
Exhaust Ports

The purpose of this report is to document the final results and conclusions of work on the behavior of aluminum titanate materials in a diesel engine environment.

Aluminum titanate materials from three different manufacturers showed significant differences in strength, stability and thermophysical properties. One material was low density with low strength, modulus and conductivity. The second material exhibited degradation to a -Al_2O_3 after aging at temperatures greater than 1000°C. The third material had very high strength as received but showed a strength loss of up to 40% after aging. However, the strength for this material after aging remained greater than the as-received strength of the other two materials.

Casting studies showed that cast-in-place ports can be produced. The most promising results were seen when the core sand composition was 50% SiC/50% Fe. The composition had thermal expansion characteristics which kept the core sand in contact with the aluminum titanate port during solidification and cooling of the cast iron.